MECHANISMS OF DECADAL CLIMATE VARIABILITY ASSOCIATED WITH THE ATLANTIC MERIDIONAL OVERTURNING CIRCULATION

A Thesis

by

LAUREN ELAINE REPLOGLE

Submitted to the Office of Graduate and Professional Studies of
Texas A&M University
in partial fulfillment of the requirements for the degree of

MASTER OF SCIENCE

Chair of Committee,	Benjamin Giese
Committee Members,	Ping Chang
	Andrea Mask
Head of Department,	Shari Yvon-Lewis

August 2018

Major Subject: Oceanography

ABSTRACT

To further identify physical mechanisms responsible for decadal climate variability, a combination of ocean reanalyses and coupled climate models were used. A pronounced trend is observed in the first EOF of SST that exhibits a spatial pattern of increasing global temperatures. An analysis of SST, the atmospheric meridional mass streamfunction, and precipitation minus evaporation illustrates a weakening Hadley circulation consisting of an expanded Northern Hemisphere Hadley cell, contracted Southern Hemisphere Hadley cell, and strong Southern Hemisphere Ferrell cell. There is also pronounced decadal variability that exhibits a prominent meridional and latitudinal temperature structure, an expanded Southern Hemisphere Hadley cell, and a poleward shift of the Northern Hemisphere Hadley circulation. This variability resembles a La Niña-like pattern that occurs in both the reanalysis, and the coupled model. As a consequence of tropical Pacific temperature variability, the Hadley circulation influences extratropical atmospheric circulation in the North Pacific and Atlantic Oceans via an atmospheric teleconnection. A correlation analysis shows a connection between the North Atlantic Oscillation Index and tropical Pacific Ocean temperature, with the Pacific Ocean SST leading by 19 months. North Atlantic related wind patterns force buoyancy changes in deep water formation regions and wave propagations along the western boundary of the North Atlantic Ocean. Thus, it is proposed that SST in the tropical Pacific Ocean forces atmospheric circulations in the North Atlantic Ocean that influence decadal variability in North Atlantic circulations.

DEDICATION

I dedicate this thesis to my parents, Brian and Karen Replogle, who have always encouraged me to pursue my dreams. I have come so far in life because of your love and support.

ACKNOWLEDGMENTS

I would like to thank my committee chair, Dr. Ben Giese, for his gracious support, guidance, and patience throughout the course of this research. Due to his assistance, I have acquired a prodigious amount of knowledge and skill sets in field of Physical Oceanography for which I will always be grateful. I would additionally like to thank my committee member Dr. Ping Chang for his support throughout this research and, most importantly, furthering my graduate education by bridging the gap between Oceanography and Atmospheric Sciences. Lastly, I would like to extend my upmost appreciation to my committee member and upcoming supervisor at the Naval Oceanographic Office, Dr. Andrea Mask. Thank you for your guidance in this research and especially for the opportunity to advance my education and forthcoming career with the United States Navy. You have undoubtedly assisted in making my dreams a reality by providing the opportunity to use my knowledge in Physical Oceanography and Meteorology to support the missions of the United States Navy. I will forever be greateful.

I would like to thank my friends, faculty, staff in both the Atmospheric Science and Oceanography Departments for supporting my undergraduate and graduate career at Texas A&M University. I will always cherish my time at Texas A&M thanks to the friends made and the department professors.

I would like to further thank my parents, Brian and Karen Replogle, for their support in furthering my college education and always encouraging me to reach for the stars. I wouldnt be this far in life without your love and guidance. I also want to show my appreciation to my brothers Dustin and Reece for standing beside me along this journey in my life. Lastly, I would like to thank my life-long companion, Barrett Goudeau, for your love, encouragement, and support by walking along side me in my graduate career.

CONTRIBUTORS AND FUNDING SOURCES

This work was supported by a thesis committee consisting of Professor Benjamin Giese and Professor Andrea Mask of the Department of Oceanography and Professor Ping Chang of the Department of Atmospheric Sciences.

Graduate study was supported by a fellowship from the United States Department of Defense Science, Mathematics And Research for Transformation (SMART) Scholarship for Service Program and from the National Science Foundation (NSF) Scholarships in Science, Technology, Engineering, and Mathematics (S-STEM) program hosted by the Department of Oceanography at Texas A&M University.

NOMENCLATURE

AMOC	Atlantic Meridional Overturning Circulation
CAM	Community Atmosphere Model
CCSM	Community Climate System Model
CESM	Community Earth System Model
CICE	Los Alamos Sea Ice Model
CISM	Community Ice Sheet Model
CLM	Community Land Model
DWBC	Deep Western Boundary Current
ENSO	El Niño-Southern Oscillation
EOF	Empirical Orthogonal Function
GFS	Global Forecasting System
ITCZ	Intertropical Convergence Zone
MMS	Meridional Mass Streamfunction
MOC	Meridional Overturning Circulation
NADW	North Atlantic Deep Water
NAO	North Atlantic Oscillation
NCAR	National Center for Atmospheric Research
NECC	North Equatorial Counter Current
NH	Northern Hemisphere
OHT	Ocean Heat Transport
PC	Principle Component
PDO	Pacific Decadal Oscillation

PNA	Pacific-North American
POP	Parallel Ocean Program
RAPID-MOCHA	Rapid Climate Change-Meridional Overturning Circulation and Heatflux Array
SH	Southern Hemisphere
SLP	Sea Level Pressure
SODA	Simple Ocean Data Assimilation
SST	Sea Surface Temperature
WES	Wind-Evaporation-Sea surface temperature

TABLE OF CONTENTS

Page

LIST OF FIGURES

1. INTRODUCTION

Through its transport of heat and freshwater, the Atlantic Meridional Overturning Circulation (AMOC) is a part of the global thermohaline circulation that plays a central role in the past, present, and future climate. The circulation involves interactions between northward flowing surface currents, southward flowing deep currents, and regions of water mass transformation as depicted in Figure 1. Beginning in the southern Atlantic Ocean, near-surface currents flow northward along the western coast of Africa until a portion of the water encounters the westward-flowing equatorial currents (Garzoli and Matano, 2011). The equatorial currents flow across the ocean basin and eventually merge with the Gulf Stream, which is known for its warm northward-flowing currents. The Gulf Stream flows along the eastern boundary of North America until it separates near Cape Hatteras into a meandering jet to the northeast. These warm waters extend into the North Atlantic Current that ultimately intersects with the Labrador Current, a cold southward-flowing current (Rossby, 1999).

As the North Atlantic Current migrates northward into the Nordic and Labrador Seas of the North Atlantic Ocean, buoyancy loss and mixing occur. As a result, the surface waters become colder and denser, which causes the water to sink to depths down to 4 km (Marshall and Schott, 1999). In these regions, deep water formation occurs, which is a major driver of AMOC return flow. In these formation areas, the deep convection and overflow of dense water create the cold southward flowing North Atlantic Deep Water (NADW). The NADW exports water out of the deep convection zones through the Deep Western Boundary Current (DWBC). The resulting current flows along the western basin of the Atlantic Ocean, across the equator, and eventually into the Southern Ocean (Bower et al., 2009). To balance the export of the DWBC, the inflow of warm near-surface waters from the Indian and Pacific Oceans and wind-induced upwelling of dense water of the Antarctic Circumpolar Current combine with the eastern currents in the South Atlantic to begin the global circulation over again.

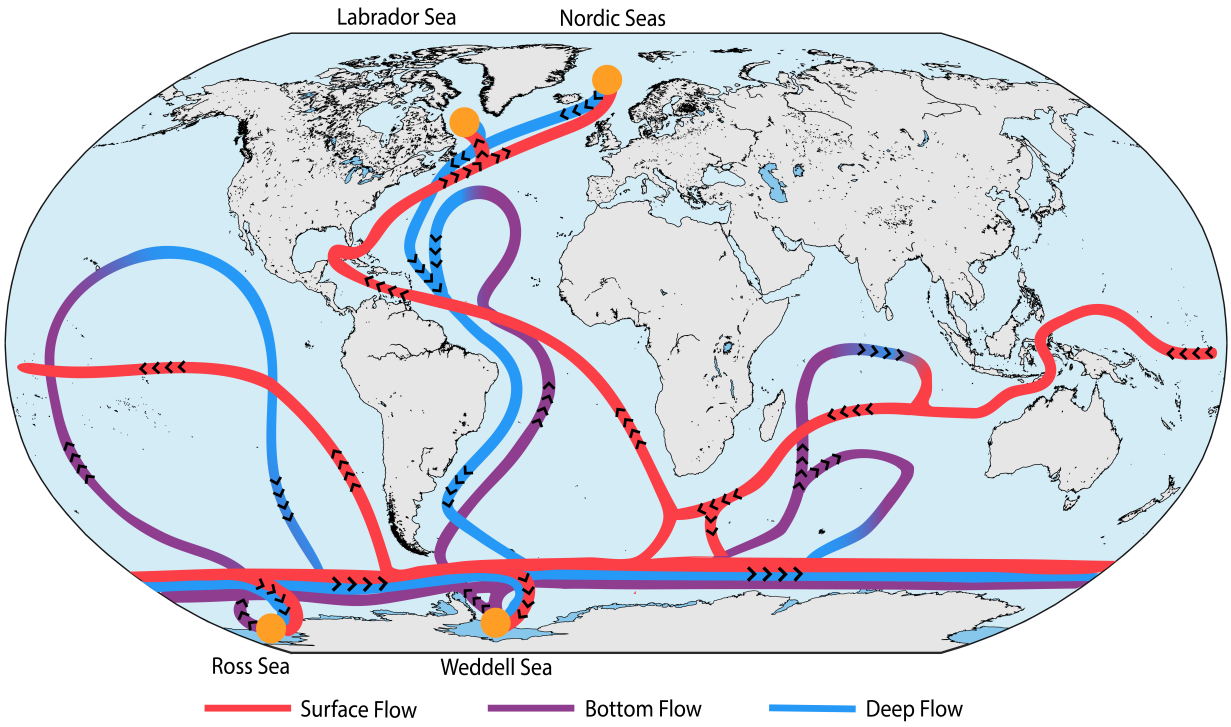

Figure 1: A simplified schematic of the global overturning circulation. Warm near-surface currents (red lines) originating in the South Ocean flow across the Atlantic into the Nordic and Labrador Seas. Deep Water Formation (orange circles) results in a cold southward-flowing deep western boundary current (blue lines) that travels into the South Ocean. Figure based on schematic by Kuhlbrodt et al. (2007)

The elaborate circulation of the Atlantic Ocean plays a significant role in understanding the role of AMOC and its importance in climate. The entire circulation is the primary contributor to ocean heat transport (OHT) from the South Atlantic, across the equator, and into the polar regions of the North Atlantic Ocean. It is thought that AMOC strength and OHT have global impacts that include setting the position of the Intertropical Convergence Zone (ITCZ; i.e., a narrow belt of clouds located approximately six degrees north of the equator thats comprised of thunderstorm activity Schneider et al., 2014), reducing anthropogenic greenhouse gasses in the atmosphere, and supplying heat to the atmosphere that drive atmospheric circulations and climate patterns (Gulev et al., 2013; Kostov et al., 2014; Marshall et al., 2013; Trenberth and Caron, 2001). Observations, proxies, and numerical model studies have provided links between AMOC variability and global

climate patterns.

As technology advanced, concerns about the changing climate spurred new research, which revealed unprecedented effects of global warming caused by anthropogenic carbon dioxide. Early numerical model studies suggested that a slowdown and potential shutdown of AMOC could occur as a result of global warming (Manabe et al., 1990; Washington and Meehl, 1989). Since AMOC plays an important role in atmosphere and ocean patterns, the implied consequences on the global climate as a result of a drastic slowdown of AMOC are important. Potential effects of a slowdown could be a colder Arctic, increases in the total Arctic ice mass, a southward shift of the Intertropical Convergence Zone, weakening of Asian and Indian monsoons, reduction in North Atlantic uptake of atmospheric carbon dioxide, and changes in Atlantic storm tracks and rainfall frequency (Chiang and Bitz, 2005; Schuster and Watson, 2007; Stouffer et al., 2006; Vellinga and Wood, 2002). With these potentially detrimental effects, numerical models have been developed to predict and understand the future of global climate. Unfortunately, models can contain errors in estimating AMOC variations and its associated implications for a multitude of reasons.

Ocean hindcasts and forecasts use observations to make inferences on the past and future strengths of AMOC. Because there is a lack of spatial and temporal resolution of observational data, numerical models have difficulty representing AMOC strength (Buckley and Marshall, 2016). For example, Coupled Model Intercomparison Project Phase 5 (CMIP5) models have provided estimates of the maximum mean strength of AMOC to occur range from 13 Sv at 20°N to 31 Sv at 60°N (Zhang and Wang, 2013). Although improvements of strength estimates through data assimilation reduce error, there are still models that disagree with them. The annual and seasonal variability of ocean heat transport and AMOC strength are underestimated in multiple model reanalysis studies (Munoz et al., 2011). This suggests that current observational programs are not adequate in correcting all model errors. Nonetheless, the majority of models can still reproduce similar trends that are present in observations from the RAPID mooring array program (Hirschi et al., 2013). It's inferred that this achievement is due to defining in the models that the atmosphere is the driving process of AMOC, such as the wind strength and direction.

Overall, the timing, magnitude, location, and depth patterns of AMOC differ substantially between models. Although observations are thought to create a substantial agreement between AMOC estimates, the trends found in model approximations depend on the time frame of the analysis, assimilation technique, and input parameters for the numerous ocean models. The need for model improvements requires additional observations, standard parameterization, and enhanced assimilation techniques to advance evaluations of AMOC and its variability (Buckley and Marshall, 2016).

Early observational estimates of AMOC began with utilizing trans-Atlantic hydrographic sections and currents determined by satellite and land-based wind observations. One difficulty in using this method concerns the assessment of narrow and deep boundary currents. The addition of Argo floats and satellite altimetry—which provides sea surface height—aids estimations. However, due to limited temporal resolution, the use of these techniques was insufficient in assessing the variability of AMOC. The lack of historical data ultimately led to the development of a continuous observational array.

The Rapid Climate Change-Meridional Overturning Circulation and Heatflux Array (RAPID-MOCHA) was the first continuous observational program dedicated to monitoring the strength of AMOC and Atlantic OHT. Starting in March 2004, the mooring array spans across the Atlantic Ocean at 26.5°N, where it consistently monitors temperature, salinity, and current speeds from the sea surface to the ocean floor (Rayner et al., 2011). Data collected from the array is capable of measuring AMOC variability, as shown by McCarthy et al. (2012). For the first five years of observations, the daily and seasonal strength varied little from the average circulation strength of 18.5 Sv (Figure 2). The constituent components that make up the circulation, the Gulf Stream, Ekman transport, and the upper mid-ocean transports, varied little in that period as well. Then at the beginning of 2009, AMOC strength declined below the mean value and remained weak until mid-2010. The long-term change represented a reduction of strength by 30%. This is thought to be caused by a deepening of the overturning circulation, strengthening of the DWBC, and a reduction in the Ekman transport (McCarthy et al., 2012).

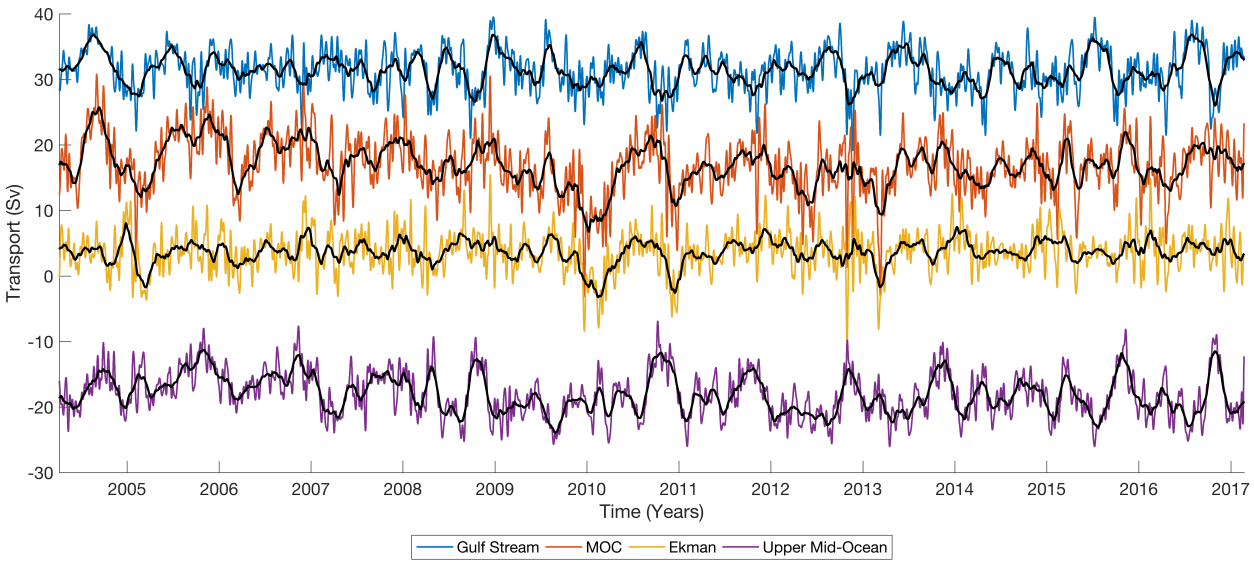

Figure 2: A time series of daily (colors) and three-month (black) low-pass filter for the Gulf Stream transport (blue), Meridional Overturning Circulation (MOC) transport (red), Ekman transport (yellow), and upper mid-ocean transport (purple) from April 2004 to February 2017. Data from the RAPID-MOCHA monitoring project is provided Smeed et al. (2017)

The success of the RAPID array has led to multiple mooring arrays across the Atlantic Ocean, from the Labrador Sea in the deep-water formation zones to the South Atlantic, with the goal of observing the deep western boundary current and circulations south of the equator. Data from the various array locations contribute to understanding AMOC through numerical model assimilations and data analysis. Although they provide continuous observations, there is a historical lack of temporal and spatial resolution that is needed to provide substantial evidence of annual trends and to shed light on the causes of decadal variability.

Model studies have been utilized to explore AMOC variability on a range of timescales, where mechanisms of variability are strongly dependent on the timescale. On short timescales, models can estimate and reproduce much of the large interannual variability of AMOC that is observed by the RAPID array at 26.5°N. This is thought to be due to AMOC responding primarily to atmospheric forcing through wind stress and the associated Ekman transport response. Roberts et al. (2013) found that 70-80% of AMOC variability can be reproduced in

ocean models if they are driven by wind stress. These results did not require data assimilation, thus highlighting the importance wind has in generating a high-frequency response of the upper ocean and the stratification. In contrast, low-frequency (decadal to multidecadal) variability is thought to be driven by geostrophic circulation changes (Hirschi et al., 2007).

Modeling historical AMOC changes on longer timescales poses challenges since the observational records are too short to validate low-frequency variability and the dominant signals contained in different models. In general, ocean hindcast experiments with a variety of atmospheric boundary conditions show increasing trends of AMOC in the 1980s to mid-1990s followed by decreasing trends (Bentsen et al., 2004; Böning et al., 2006; Danabasoglu et al., 2016; Häkkinen, 1999; Robson et al., 2012). Before the 1980s, models tend to have a wide range of AMOC trends. It is important to note that depending on the period of analysis, specific model, and assimilation technique, AMOC and OHT trends vary across model experiments indicating that AMOC estimates are sensitive to assimilation techniques.

On decadal timescales, models exhibit meridionally coherent modes of North Atlantic MOC and OHT variability (Danabasoglu, 2008; Delworth et al., 1993; Knight, 2005). However, the exact timescale at which AMOC and OHT are meridionally coherent is not fully understood but is thought to originate from subpolar regions and reflect a response to time-dependent buoyancy forcing (Böning et al., 2006; Robson et al., 2012; Yeager and Danabasoglu, 2014). It is thought that the buoyancy fluctuations are driven by North Atlantic Oscillation (NAO) forcing over the subpolar regions such as the Labrador Sea (Bentsen et al., 2004; Delworth and Zeng, 2016; Kim et al., 2018; Robson et al., 2012). NAO-related wind stress impacts the subpolar gyre circulation which plays an important role in the deep-water formation of AMOC. During a positive phase of NAO, the atmosphere extracts heat from the subpolar gyre resulting in increased deep-water formation in the Labrador Sea, horizontal density gradients, and thus the strength of AMOC (Delworth and Zeng, 2016; Yeager and Danabasoglu, 2014).

Another feature associated with AMOC low-frequency variability is basin wide fluctuations in North Atlantic SST, namely the Atlantic Multidecadal Variability (AMV; Knight, 2005) . AMV is

thought to be a mode of variability associated with slow ocean processes caused by AMOC variability, however, no observational study has successfully proven that there is a link between SST and AMOC variability (Lozier, 2010). The relative roles of external forcing in creating decadal SST anomalies has not been clearly identified, and is thought to be a result of internal atmospheric and oceanic processes (Knight, 2009). The hypothesis that AMOC plays an important role in decadal SST anomalies has led to numerous model studies. Some model results suggest that SST anomalies are a result of AMOC variability (Häkkinen, 1999; Knight, 2005; Roberts et al., 2013), whereas other studies suggest SST anomalies are a result of other processes such as local atmospheric forcing and Rossby waves (Buckley et al., 2012; Danabasoglu, 2008). Since it has been shown that the AMV has also shown to be related to changes in the subtropical and subpolar gyres, Schneider and Fan (2012) concludes that mean gyre circulation is needed to explain Atlantic SST variability, thus involving the NAO. This relation implies that AMOC, SST, and NAO play a role in decadal ocean dynamics.

Much of the existing literature describes AMOC variability as being forced in the North Atlantic Ocean. However, it possible that AMOC variability may be forced from outside of the North Atlantic Ocean. Dong et al. (2011) suggest that changes in AMOC at 34°S are a response to ocean exchanges between the Pacific and Indian Oceans, near Cape Agulhas. Biastoch et al. (2008) demonstrated that this region acts as a leakage from the Indian Ocean to the Atlantic Ocean and is a source of decadal variability of AMOC. Low-frequency undulations of thermocline depth propagate from the Agulhas region and travel across the South Atlantic as a Rossby wave and then northward along the western boundary of the North Atlantic Ocean as a Kelvin wave. Delworth and Fanrong (2012) suggest that centennial variability in AMOC is related to propagation of salinity anomalies from the Southern Ocean to the subpolar regions of the North Atlantic Ocean.

Since AMOC plays a central role in climate, it is important to understand what mechanisms set the low-frequency variability of the ocean circulation. On interannual to decadal timescales, AMOC fluctuations are primarily caused by geostrophic and related buoyancy anomalies on the

western boundary of the North Atlantic Ocean. Since the air-sea flux is complex, it is important to decipher the external and internal forces related to AMOC variability and further identify mechanisms interacting with the North Atlantic Ocean basin.

In this study, AMOC variability is explored in an ocean reanalysis as well as in a global coupled model. To interpret AMOC responses between internal and external forcing, an additional coupled model is used that only contains pre-industrial forcing. The goal is to identify physical mechanisms and natural/external forcings that are associated with decadal variability seen in AMOC. To achieve this goal, EOF analyses and regressions are conducted with oceanic and atmospheric variables that are then correlated to the low-frequency signal in AMOC.

2. MODEL DESCRIPTIONS

One of the ocean models used for the analysis of this paper is a version of the Simple Ocean Data Assimilation system with sparce observational input (SODAsi) and is described in detail by Giese et al. (2016). The 8-member ensemble ocean reanalyses uses the Simple Ocean Data Assimilation (SODA) methodology that relies on the Parallel Ocean Program (POP; Smith et al., 1992) ocean model and the SODA data assimilation algorithm (Carton and Giese, 2008). The POP ocean model has a resolution of $0.4^\circ \times 0.25^\circ$ with 40 vertical levels. The model covers the globe with a distorted grid in the Northern Hemisphere (NH). Displacing the North Pole avoids the convergence of meridians in order to resolve the Arctic Ocean. The resolution of the meridional dimension increases poleward to reduce grid distortions due to convergence of longitudes at high latitudes. The algorithms used are the same as for earlier versions of SODA, however the data used is different. In SODAsi.3, SST observations obtained from International Comprehensive Ocean-Atmosphere Data Set (Woodruff et al., 2010) are assimilated. The assimilation technique follows Carton and Giese (2008), where assimilation of the observations are completed through a sequence of a 10-day update cycle, where at the end of the procedure, the model generates 5-day averages of variables mapped onto a uniform $0.5^\circ \times 0.5^\circ$ grid.

An important aspect of SODAsi.3 is that it's loosely-coupled to an atmosphere reanalysis. The loosely-coupling is achieved by first running SODA forced with the 20^{th} Century Reanalysis Version 2 (20CRv2; Compo et al., 2011) atmospheric model, forming SODAsi.2. Using SST from SODAsi.3, 20CR Version 2c (20CRv2c) was formed and used for forcing SODAsi.3 (Giese et al., 2016). The first integration of the coupled analysis of SODAsi.3 uses 18 ensemble members from SODAsi.2 that used boundary conditions from 20CRv2 from 1948-2011. Prior to 1948 (from 1846 to 1947), an experimental version of 20CR was used, calling the combined version 20CRv2b. The boundary conditions for SST and sea ice concentration for 20CRv2 are provided by the Hadley Centre Global Sea Ice and Sea Surface Temperature Version 1.1 data set (Rayner, 2003) and is also used in 20CRv2b from 1871 to 1947. For the second iteration for the coupled system, SST

from SODAsi.2 is used in 20CRv2c for the period 1846-2013.

Given that 20CRv2c atmosphere model is integrated into the forcing of SODAsi.3, it was used to obtain the data used in the analysis of the atmosphere and explained in detail by Compo et al. (2011). Briefly, the atmospheric-land model is based on the National Centers for Environmental Prediction (NCEP) Global Forecasting System (GFS) atmosphere model. It is derived from using only synoptic surface pressure observations and monthly SST, and sea-ice distribution as the boundary conditions. The analysis for 20CRv2 has a spatial resolution of nearly 200 km on an irregular Gaussian grid in the horizontal, and 28 hybrid sigma-pressure levels in the vertical. The assimilation procedure used is based on an Ensemble Kalman Filter and based on the Ensemble Square Root Filter algorithm (Compo et al., 2006, 2011; Whitaker and Hamill, 2002). The model generates an ensemble of 56 nine-hour forecasts and produces 56 six-hourly analysis data sets. The 20CRv2c ensemble mean will be used for this study, because it provides reanalysis data for 1851 to 2014, which can be compared with SODAsi.3.

To determine the associated changes in decadal variability of AMOC due to internal versus external forcing, a control experiment was created using the National Center for Atmospheric Research (NCAR) Community Earth System Model version 1.0 (CESM1; Hurrell et al., 2013). CESM is a fully-coupled model that consists of atmosphere, cryosphere, land, and ocean components that communicate through a fixed coupler. For this configuration, all components of the model are fully active and coupled to each other using the CESM flux coupler version 7. The experiment uses the Community Atmosphere Model Version 5 (CAM5; Neale et al., 2010) for the atmosphere model, Parallel Ocean Program Version 2 (POP2; Danabasoglu et al., 2012) for the ocean model, and the Community Land Model (CLM; Lawrence et al., 2011) for the land model. Futhermore, POP2 contains 60 vertical levels, with greatest resolution in the upper ocean where the resolution is in 10-m increments in the upper 160 m of the ocean. The remaining constituents of the model include the sea-ice component using the Los Alamos sea ice model (CICE; Hunke et al., 2010), and the stubbed land-ice component using the Glimmer-Community Ice Sheet Model (Glimmer-CISM; Hurrell et al., 2013). The experiment ran with a $0.9^{\circ} \times 1.25^{\circ}$ resolution

for the atmosphere and land models, and $1^\circ \times 1^\circ$ for the ocean and ice models.

To create the control experiment, CESM is integrated for 843 years with preindustrial forcing and fixed carbon dioxide (CO_2) at a 1° horizontal resolution. The preindustrial period, also known as pre-1850, describes a climate state before human activities started changing the environment through fossil fuel combustion. With preindustrial forcing, the control experiment can capture natural forcing without the influence of anthropogenic climate change. The initial CESM run is retained as a startup run for the final experiment. Using initial state from the previous run, the model is integrated for 200 years to establish a control run that is used for the analysis in the study. Therefore, any reference to control refers to the preindustrial forced and fully coupled CESM from the final experiment.

The main focus of implementing the control run is to analyze Pacific Ocean internal variability through SST. Relevant details using the predecessor of CESM, the Community Climate System Model version 4 (CCSM4; Gent et al., 2011), is mentioned to establish fidelity of the model since its configured with similar components as CESM. Deser et al. (2012) provides evidence that CCSM4 simulates a realistic Pacific Decadal Oscillation (PDO; Zhang et al., 1997) and a rather realistic spatial structure of El Niño-Southern Oscillation (ENSO), with well generated ENSO-related teleconnections. However, CCSM4 overestimates the magnitude of ENSO by 30%.

3. DATA AND METHODS

SODAsi.3 contains 8 ensemble members, however, the ensemble mean at a monthly temporal resolution was used for the analysis. Data was collected from 1851-2013 and smoothed to a $1^\circ \times 1^\circ$ resolution to reduce noise from small scale geophysical flows, such as eddies. The latitudinal extent ranges from 80°S to 80°N to focus on the tropics, extra-tropics, and mid-latitude dynamics. Variables collected from SODAsi.3 include: (1) the zonal and meridional wind component (taux and tauy); (2) zonal and meridional surface current velocities (u and v); (3) sea surface temperature; (4) salinity; and (5) density.

With 56 ensemble members, atmospheric variables were assembled from 20CRv2c using the ensemble mean at a daily or monthly frequency based on data availability. If components were collected using daily averages, they were calculated into monthly averages for consistency. Based on the desired variable, the spatial coverage is provided on a regular 2° latitude $\times$ 2° longitude grid or a T62 Gaussian grid. The environmental variables collected include: (1) the zonal and meridional wind component (u and v); (2) precipitation and evaporation (P$-$E) rate; (3) mean sea level pressure (SLP); and (4) omega. To identify natural variability, the CESM control experiment was used and explained in Section 4.1.2, where 200-years of monthly global sea surface temperature was collected. Lastly, the index for the North Atlantic Oscillation (NAO) is obtained from 1851 to 2013 from Jones et al. (1997).

To objectively analyze decadal variability of sea surface temperature and its relation to AMOC, SST from SODAsi.3 and CESM was used to calculate an Empirical Orthogonal Function (EOF). In performing the EOF analysis, unfiltered monthly departure fields (SST*) were calculated. This is defined as departures of the local anomalies from the concurrent global field; for example, in Equation (1):

$$\text{SST}^* = SST - [SST] \tag{1}$$

Where [-] denotes the global average of the field at each grid point for the same month. In other

words, the anomaly field is calculated by taking the original data and subtracting the long term mean for each month at each grid point to receive monthly departure fields. In formulating the data matrix for the EOF analysis, the data at each grid point is weighted by the square root of cosine of latitude shown in Equation (2):

$$\sqrt{cos(\phi)} \tag{2}$$

This allows the variance at each grid point to be weighted in proportion to the area of the grid box. The datum is then standardized to the unit variance. In displaying time series, a 5-year boxcar smoothing filter was applied to reduce high-frequency variability caused by seasonal and annual noise. If missing data existed, not a number (NaN) was used in the analysis.

The EOF analysis provides the temporal pattern through calculation of expansion coefficient time series of the data, which is also referred to as the principle components (PC). The EOF spatial patterns are generated by regressing the monthly fields onto their respective principle components. The amplitudes that appear on an EOF spatial map represent the amplitude of the field deviations for that variable. In displaying the time series and computing the correlation coefficients, the resulting times series that is padded with the first and last values is removed.

Regression maps and time series documenting decadal variability of SST were obtained to draw correlations between SST and atmospheric and oceanic variables. To create a regression map, the variables were regressed onto the expansion coefficients of SST. Variables that were regressed include the wind components, the surface current components, salinity, density, mean sea level pressure, the atmospheric mass streamfunction, and omega. Additional EOF analyses were conducted on components correlating to the principle components of SST.

To identify tropical expansion and contraction, a Joint Empirical Orthogonal Function (EOF) was used. In analyzing the zonal mean overturning circulation at all levels in the atmosphere, the zonal mean meridional mass streamfunction (MMS) at 500-mb (Equation (3) Ψ_{500}) and the zonal mean P$-$E were used in the joint analysis. The MMS was calculated as:

$$\Psi = \frac{2acos(\phi)}{g} \int_{P_o}^{P} [v] dp \tag{3}$$

Where a is the radius of the Earth, ψ is the latitude, g is the gravitational acceleration, P_0 and P is the lowest and largest pressure level given by the model, and v is the meridional wind component with brackets denoting the zonal average. Anomalies for each variable was calculated by removing the long term monthly mean and then normalized by using its standard deviation. A 5-year boxcar filter was then applied to the anomalies at each grid point to reduce noise. Since the Hadley circulation is seasonally dependent, additional anomaly fields were calculated by averaging the monthly data into boreal winter (December, January, February; DJF), spring (March, April, May; MAM), summer (June, July, August; JJA), and fall (September, October, November; SON). Lastly, the long term mean for each season was removed from the data and normalized by its standard deviation.

To describe inter-hemispheric decadal variations, the MMS anomalies were used to calculate an additional EOF analysis and the MMS resulting from Equation (3) was used to identify the strength of the atmospheric circulation and the latitude extent of the Hadley circulation. The EOF analysis was conducted as previously discussed. The intensity of the Hadley circulation is identified by locating the maximum value of the MMS in the tropics for the Northern Hemisphere and locating the minimum value for the Southern Hemisphere. Lastly, to determine the latitude extent of the Hadley cell edge, the zero-crossing of MMS was calculated between the equator and 60° for the corresponding hemisphere.

4. RESULTS

Giese et al. (2016) showed that SST fields in SODAsi.3 display a wide range of variability, with time scales ranging from interannual to decadal. Briefly, SODAsi.3 depicts a pronounced SST trend from the early 1900s to 2013. The spatial pattern of the trend shows increasing temperatures throughout most of the global oceans, with some regions of cooling. In addition to a trend, an EOF analysis of SST presents considerable multi-decadal variability; the North Atlantic exhibited this variability with an amplitude of about 0.5°C. To understand changes in SST described in the analysis, the meridional overturning streamfunction was calculated and found to be highly correlated to the spatial structure of the second EOF—where temperature change leads the streamfunction by about 9 years. In order to further understand how ocean circulation responds to SST change, we begin reproducing the EOF analysis presented by Giese et al. (2016) using SST from SODAsi.3 to verify and formulate a basis for this study.

4.1 Modes of sea surface temperature variability

4.1.1 Global Trend

An EOF analysis of SST illustrates patterns of variability contained in SODAsi.3. The analysis is performed on normalized SST anomalies that have been smoothed with a 5-year boxcar average. Three distinct modes of interannual to decadal variability are identified by the analysis. The wind anomaly accompanying each mode is displayed by projecting the zonal and meridional wind stress components onto the corresponding PCs.

The first EOF explains 53% of the variance and displays a pronounced warming trend from about 1910 to the end of the record (Figure 3). Prior to 1910, values remain relatively constant as described by a 95% student t-test. Although there is a dominant warming trend, the EOF shows considerable spatial variability. The spatial pattern has increasing temperatures throughout most of the global oceans, with some important regions of cooling. The greatest warming exists between 20°S and 40°S in the Southern Hemisphere, the western boundary of Asia, the North Pacific Ocean,

and in the North Atlantic Ocean along the western boundary of North America. At the southern tip of the African continent, an extension of the Agulhas Current from the Indian Ocean is revealed with maximum values reaching 3°C. Regions of cooling exist at the Kuroshio Current and Gulf Stream extension region, the central Pacific Ocean, equatorial eastern Pacific and Atlantic Oceans, and the Southern Ocean surrounding the continent of Antarctica. To further explore origins of changing heat, the wind stress is projected onto the first temporal component of SST.

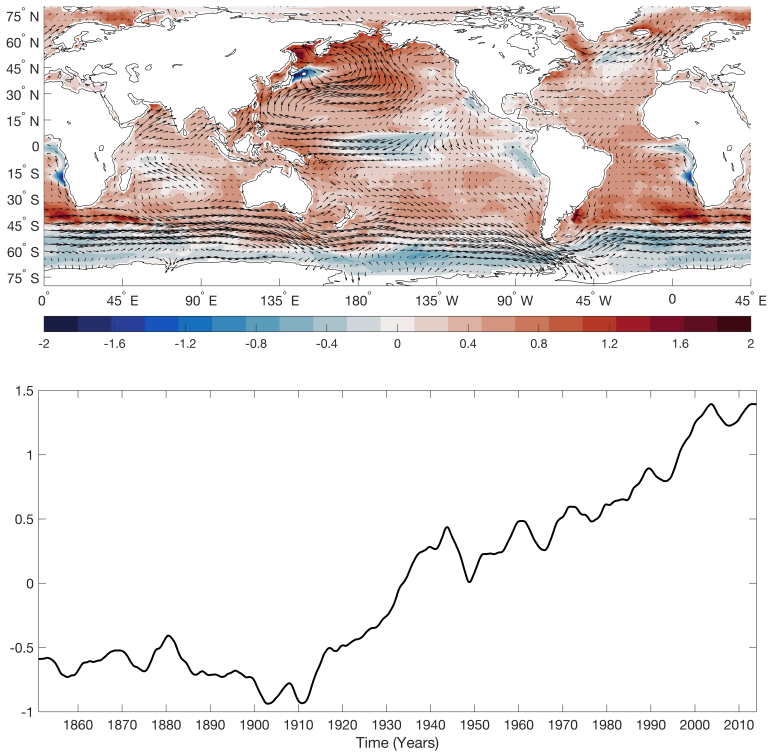

Figure 3: The spatial and temporal patterns for the first EOF of monthly SST anomalies from SODAsi.3 for the period 1851-2013. Winds are projected onto each time series as shown as vectors.

The spatial structure of SST in the tropical Pacific Ocean suggests the redistribution of heat shown by the accompanying changes in atmospheric circulation. The redistribution of heat induces atmospheric circulation fluctuations that are partially caused by changes in ocean circulation. The regions of largest wind stress change are located in the Pacific Ocean and

Southern Ocean (Figure 3). Located at the region of cooling at the equatorial Pacific Ocean, the wind stress exhibits cross-equatorial changes. In the North Pacific, there is an enhanced anticyclonic circulation thats indicative of northward migration of the Hadley cell (Giese and Carton, 1999). The Hadley cell is a low-latitude overturning circulation that consists of rising air at the equator and sinking air at $\tilde{3}0^{\circ}$. The circulation transports energy poleward to reduce the equator-to-pole temperature gradient, thus is crucial in maintaining global climate. To assess the changes in the atmosphere circulations associated with SST gradients, a joint EOF is calculated using SST anomalies from SODAsi.3 and MMS and P$-$E anomalies from 20CRv2c.

The first Joint EOF explains 85.3% of the variance, where the first EOF of SST displays the same temporal trend and spatial pattern seen in Figure 3. As before the general pattern is warming throughout the global oceans, with regions of cooling in the central tropical Pacific and Indian Oceans, eastern tropical Pacific and Atlantic Oceans, the Southern Ocean, and the North Atlantic Ocean at the subpolar gyre. The meridional gradient of SST is reflected in the spatial pattern of MMS. The NH Hadley cell expands across the equator, dominating the tropical atmospheric circulation. Compared to climatology, it is slightly contracted compared to the average latitude extent of the NH Hadley circulation, and is weaker than normal. The strength of the SH Hadley cell is slightly stronger than its counterpart but is not significant using a student t-test. Since the SH is stronger, there is an imbalance of heat and momentum flux. The result is a strong Ferrell cell to compensate for the imbalance. With the NH Hadley cell expanding into the SH and the addition of a strong SH Ferrell circulation, the resulting SH Hadley circulation is weakened and contracted.

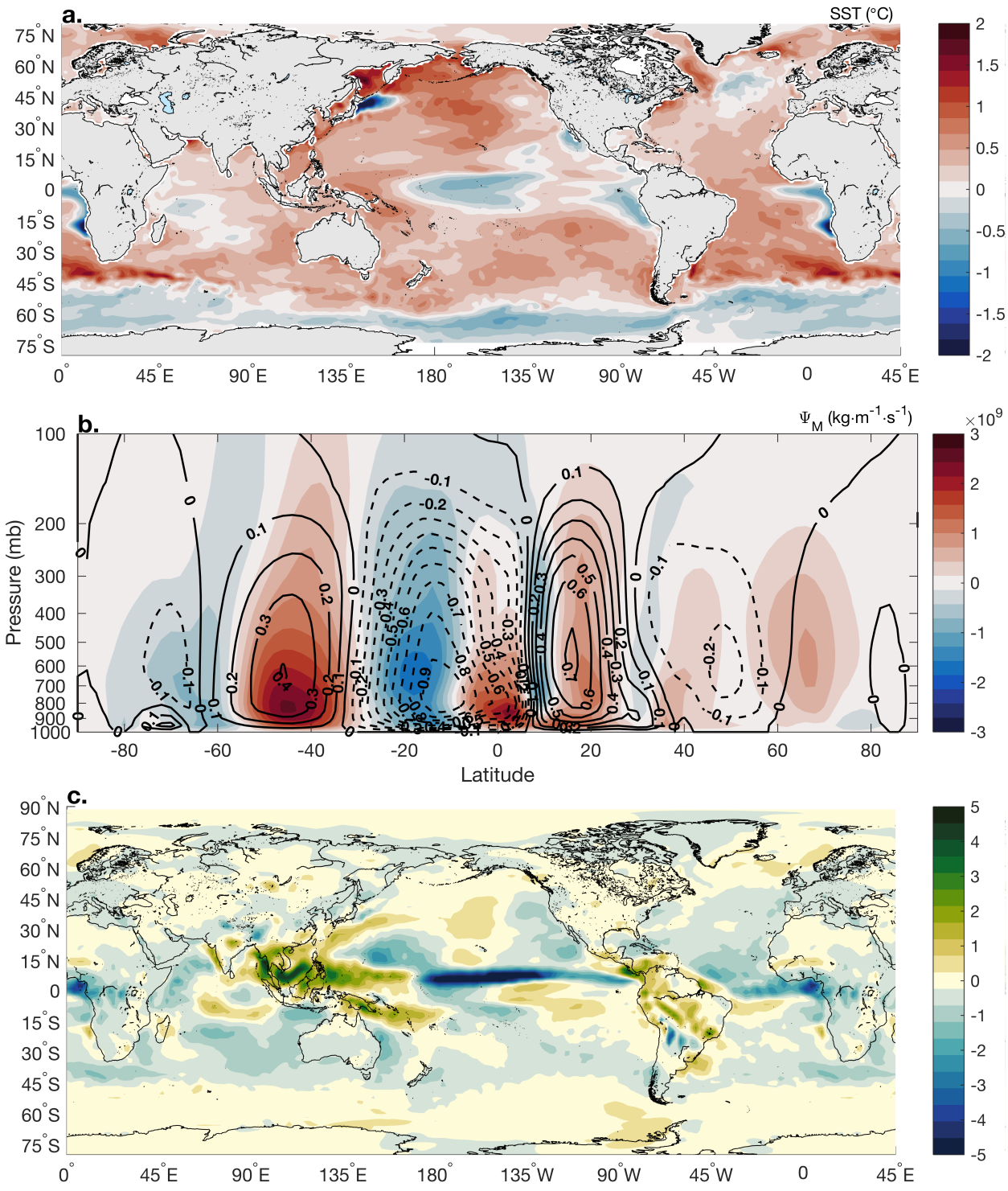

Figure 4: The first Joint EOF spatial patterns evaluated for 1851 - 2013. From top to bottom, SST anomalies from SODAsi.3, MMS anomalies from 20CRv2c and black lines representing mean climatology, and Precipitation minus evaporation (P−E) anomalies obtained from 20CRv2c. Black solid lines represent positive values of MMS and black dashed lines represent negative values of MMS. The first Joint EOF explains 85.3% of the variance. All variables have the long-term mean removed, normalized by their standard deviation, and smoothed with a 5-year boxcar average.

Additionally, the SH Hadley circulation joins the NH Hadley cell at the location of the ITCZ. The ascending motion seen at approximately 8°N is verified by the positive P−E anomalies just north of the equator, where the ITCZ is identified. The spatial structure of P−E shows that the Northern and Southern Hemispheres are similar on both sides of the ITCZ, with a region of evaporation from the ITCZ to 20° where precipitation dominates to a latitude of 40°. This is consistent with the wind stress (Figure 3), for which there are enhanced easterlies in the tropics and westerlies in the midlatitudes. Together, the warming trend depicted in the first EOF of SST and strong cyclonic wind stress in the North Pacific Ocean is consistent with a southward migration of the Hadley cell in the Northern Hemisphere and poleward expansion of the SH Hadley Cell seen in Figure 4.

To investigate the temporal variability of Hadley cell migration, the latitudinal extent of the circulation is analyzed to investigate variability in each hemisphere. Since the Hadley circulation varies largely on a seasonal basis, the edge of the circulation was calculated using seasonal means. The latitudinal extent and seasonal variability of the SH Hadley cell is shown in Figure 5. The NH Hadley cell will be discussed in section 4.1.2.

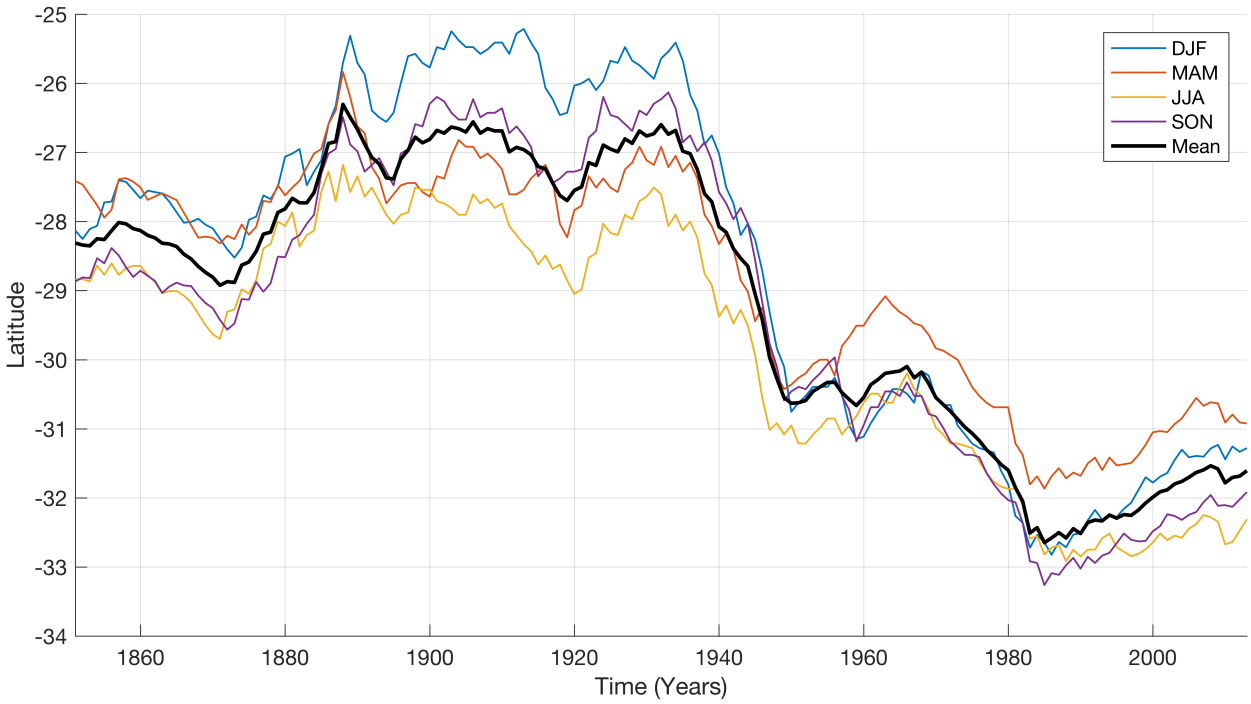

Figure 5: The latitudinal extent of the Southern Hemisphere Hadley cell, for each season from 1851-2013.

The SH Hadley cell edge does not show variability but instead shows more of a trend that indicates poleward expansion over time. The trend is consistent with the temporal component first EOF of SST, leading to external forcings such as increased greenhouse gases (Danabasoglu, 2008; Seager et al., 2010) and reduction in stratospheric ozone concentration (Kang et al., 2011) as proposed mechanisms of SH expansion. The focus of this study is to establish a relationship between SST and AMOC that exhibits decadal variability, which is not seen with the first EOF of SST. To deduce mechanisms associated with AMOC, the second EOF of SST and regression maps are created to analyze the global climate.

4.1.2 Decadal Variability

The second mode of SST (Figure 6) explains 12.4

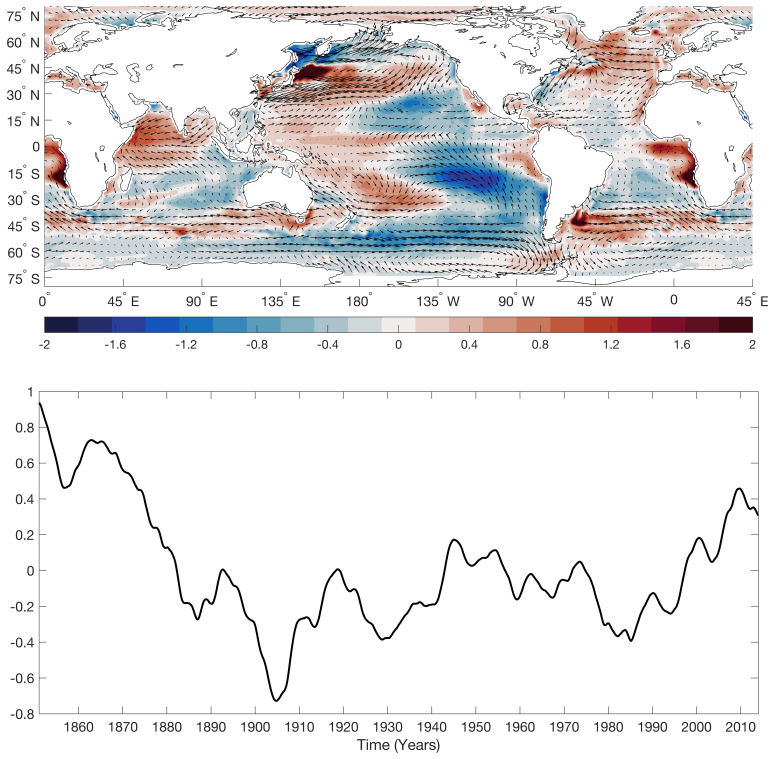

Figure 6: The spatial and temporal patterns for the second EOFs of monthly SST anomalies from SODAsi.3 for the period 1851-2013. Winds are projected onto each time series as shown as vectors.

The largest wind stress change associated with the spatial pattern of SST occurs in the Northern Hemisphere, notably over the North Pacific Ocean. The wind stress displays a cyclonic circulation thats consistent with an equatorward migration of the Hadley circulation (Giese and Carton, 1999). The wind pattern at the equator can be explained by the unique narrow band of warm anomalies that exist just north of the equator in the central tropical Pacific. The meridional gradient induces a cross-equatorial pressure gradient that strengthens the northeast trade winds and weakens the southeast trade winds, also known as the wind-evaporation-sea surface temperature (WES) feedback (Xie and Philander, 1994). Chang et al. (2006) found that the WES feedback is an important aspect in the formation and maintenance of meridional modes in the tropical oceans, with interannual SST anomalies of opposite signs existing across the equator. The WES feedback is expressed as the wind stress of the second EOF for SST (Figure 6) where there is a reduction of surface winds above the warm tongue and convergence of strong southerly

winds and weak northerly winds. The ITCZ and the ascending branch of the Hadley cell is located at the convergence of the trade winds. Thus, the second joint EOF is analyzed to assess changes in the meridional structure of the Hadley cell and the zonal mean position of the ITCZ (Gastineau et al., 2009).

The second Joint EOF (Figure 7) explains 7% of the variance and closely resembles the second EOF of SST (Figure 6); however, there are key differences. In the Pacific Ocean, a narrow band of anomalously warm SST stretches beyond the longitudinal extent of the second EOF of SST. The regions of cooling located poleward of the equatorial warm pool and in the Southern Ocean are contracted due to the addition of warm SST to the extratropical Pacific Ocean. There is warming in the eastern tropical Pacific and Atlantic Oceans, western tropical Pacific Ocean, north and south Atlantic Oceans, and the northwestern region of the Indian Ocean. As is the case for wind stress (Figure 6), the greatest change in wind is the prevailing anticyclonic circulation in the North Pacific Ocean. This pattern is indicative of a poleward migration of the Hadley cell (Giese and Carton, 1999) and is consistent with the spatial pattern of MMS in the second Joint EOF.

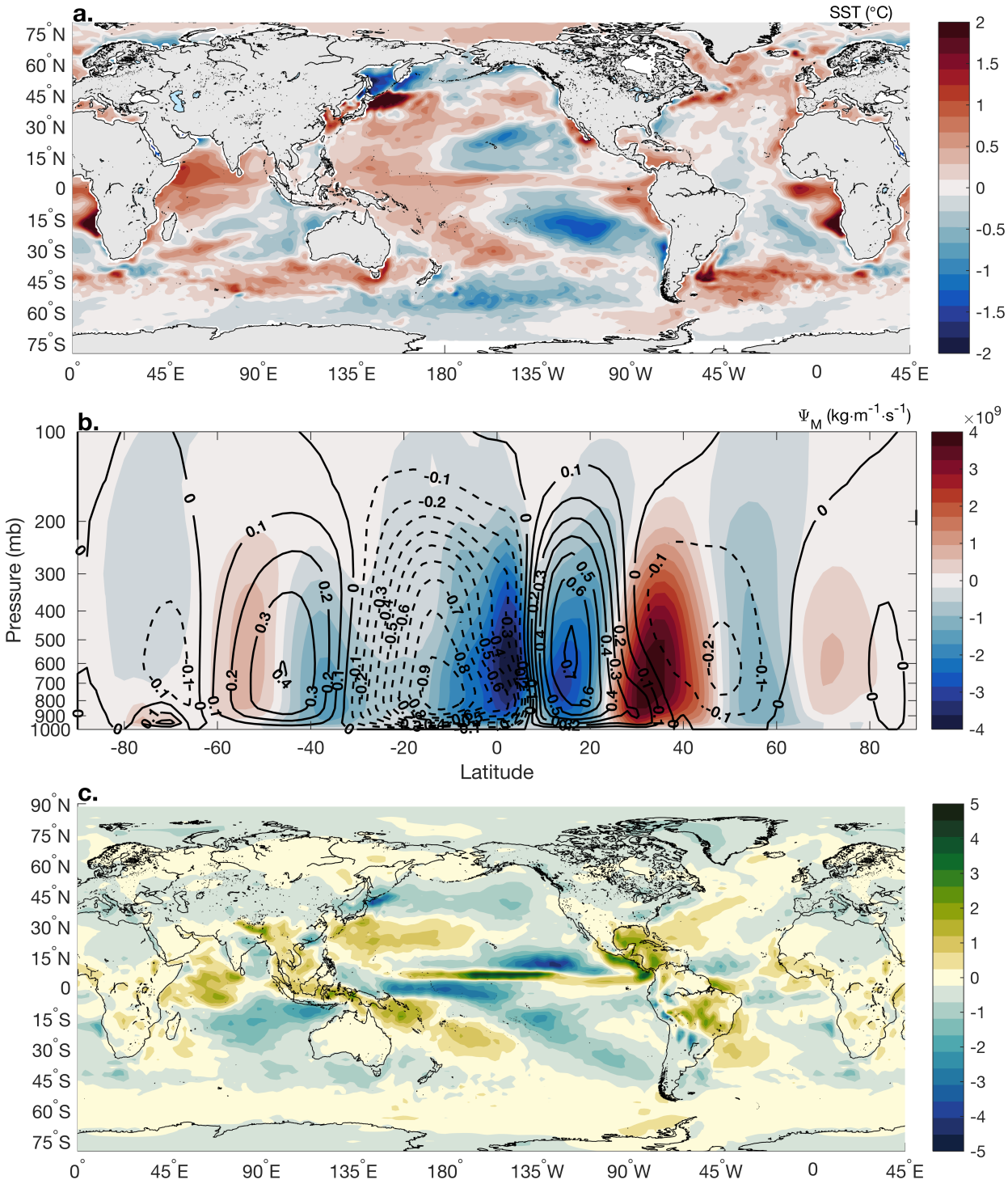

Figure 7: The second Joint EOF spatial patterns evaluated for 1851 - 2013. From top to bottom, SST anomalies from SODAsi.3, MMS anomalies from 20CRv2c and black lines representing mean climatology, and Precipitation minus evaporation (P−E) anomalies obtained from 20CRv2c. Black solid lines represent positive values of MMS and black dashed lines represent negative values of MMS. All variables have the long-term mean removed, normalized by their standard deviation, and smoothed with a 5-year boxcar average.

The SH Hadley cell extends across the equator and ranges from approximately 45°S to 8°N—beyond its climatological latitudinal extent. Persistent negative circulations at the equator, such as the structure shown in Figure 4, typically exists in boreal summer (Quan et al., 2004). However, the structure of the MMS of the second EOF presents significant distinctions from the atmospheric circulation in JJA. The SH Hadley cell is comprised of two anomalously negative circulations, a weak cell centered at 40°S and a stronger oblique cell centered just north of the equator, that join to create a broad SH Hadley cell. Adjacent to the SH Hadley cell, an additional negative circulation exists resembling the Walker circulation. This narrow circulation exhibits relatively strong motions, indicating a strong Walker circulation that typical during La Ni na (Wang, 2004). The latitudinal extent of the Walker circulation ranges from 8°N to 23°N where the NH Hadley cell begins. The NH Hadley cell expands into the midlatitudes, extending across 40°N and is remarkably strong given the magnitude of the SH Hadley cell. The combination of an enhanced SH Hadley cell and an intensified Walker circulation may be the cause for the extreme poleward expansion, whereas asymmetric SST structure across hemispheres may influence the magnitude of the circulation.

Results from the second Joint EOF of P−E further verify the anomalous circulation pattern of the atmosphere. Located at approximately 8°N, the ITCZ is apparent where large anomalous P−E values reside. The enhancement is co-located with the ascending branch of the SH Hadley cell. Since the ITCZ is located in the Northern Hemisphere, it reinforces hemispheric asymmetry in the Hadley circulation present in MMS. Just north of the ITCZ, positive values of P−E prevail in the western Pacific Ocean whereas negative values occur in eastern Pacific Ocean. The increased convection in the western Pacific Ocean and subsidence in the eastern Pacific Ocean is a consequence of intensified Walker circulation (Quan et al., 2004). Anomalous negative P−E values also exist just south of the equator, stretching across the south Pacific Ocean, and is coincident with the descending branch of the SH Hadley cell. The Northern Hemisphere displays a different pattern—the negative P−E anomalies in the North Pacific Ocean show a longitudinal structure that links to the descending motion of the NH Hadley cell. Furthermore, the pattern of

the P−E anomalies establishes a relationship between the spatial pattern of SST and MMS.

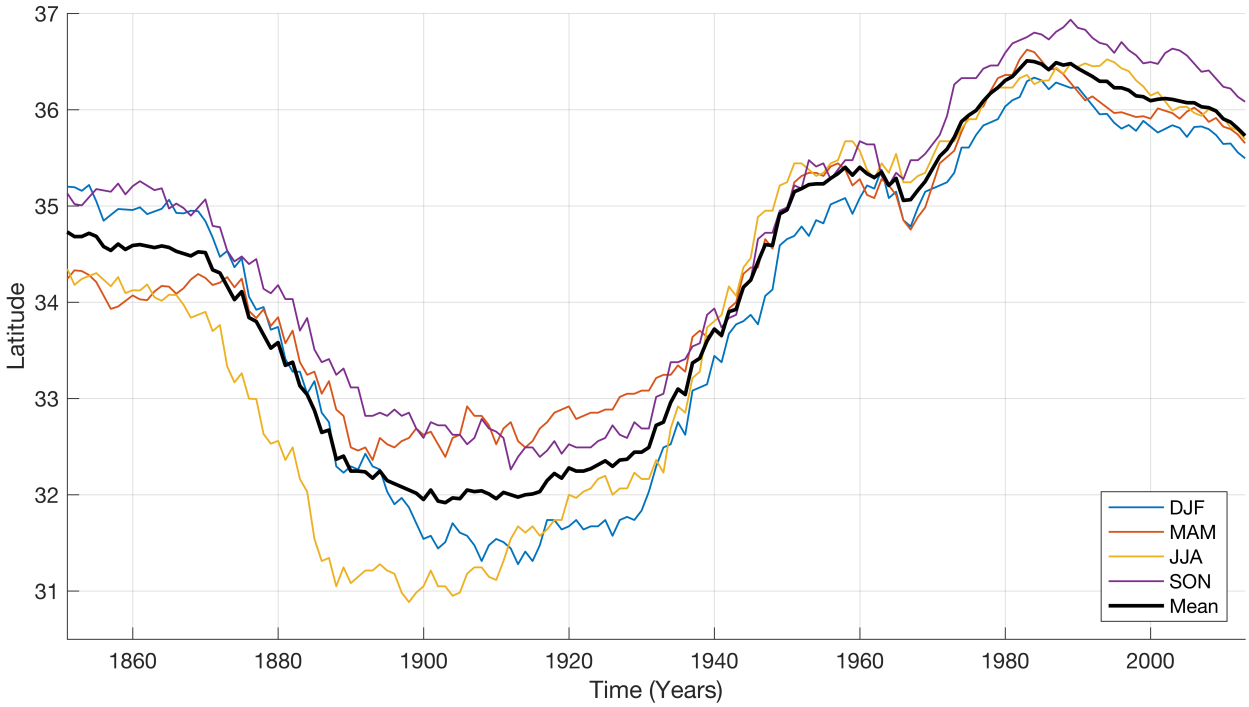

Figure 8: The latitudinal extent of the Northern Hemisphere Hadley cell, for each season from 1851-2013.

The temporal component of the latitudinal extent of the Northern Hemispheric Hadley circulation displays multi-decadal variability similar to the second principle component of SST (Figure 8). The extent of the circulation ranges from 30°N to 37°N and is nearly ubiquitous across all seasons, except for notable deviations shown by JJA in the late 19th century. A trend is not seen in the second EOF of SST or the NH Hadley cell latitudinal extent. Since the results from the first EOF displayed a trend similar to external forcing, forcing by natural factors is analyzed.

To determine the natural versus forced contributions to climate variability, an EOF analysis of SST from CESM was conducted, similar to that of SODA. This version of CESM contains fixed pre-industrial CO_2, thus, a trend as seen in SODA is not expected. As shown in Figure 9, the first EOF explains 31.7% of the variance and displays a multi-decadal pattern over time. The

largest amplitudes are observed in the Pacific Ocean at the subtropical and extratropical latitudes. Features in the Indian, Atlantic, and Southern Oceans are relatively weak, with the exception of the North Atlantic Ocean that has a small region consisting of large amplitudes off the coast of Newfoundland. Notably, the North Pacific Ocean displays the strongest amplitudes in comparison to the rest of the globe. South of the large SST anomalies, a retroflection exists at the western extent of the equatorial Pacific Ocean. These patterns in the Pacific Ocean are similar to features seen in SODAsi.3.

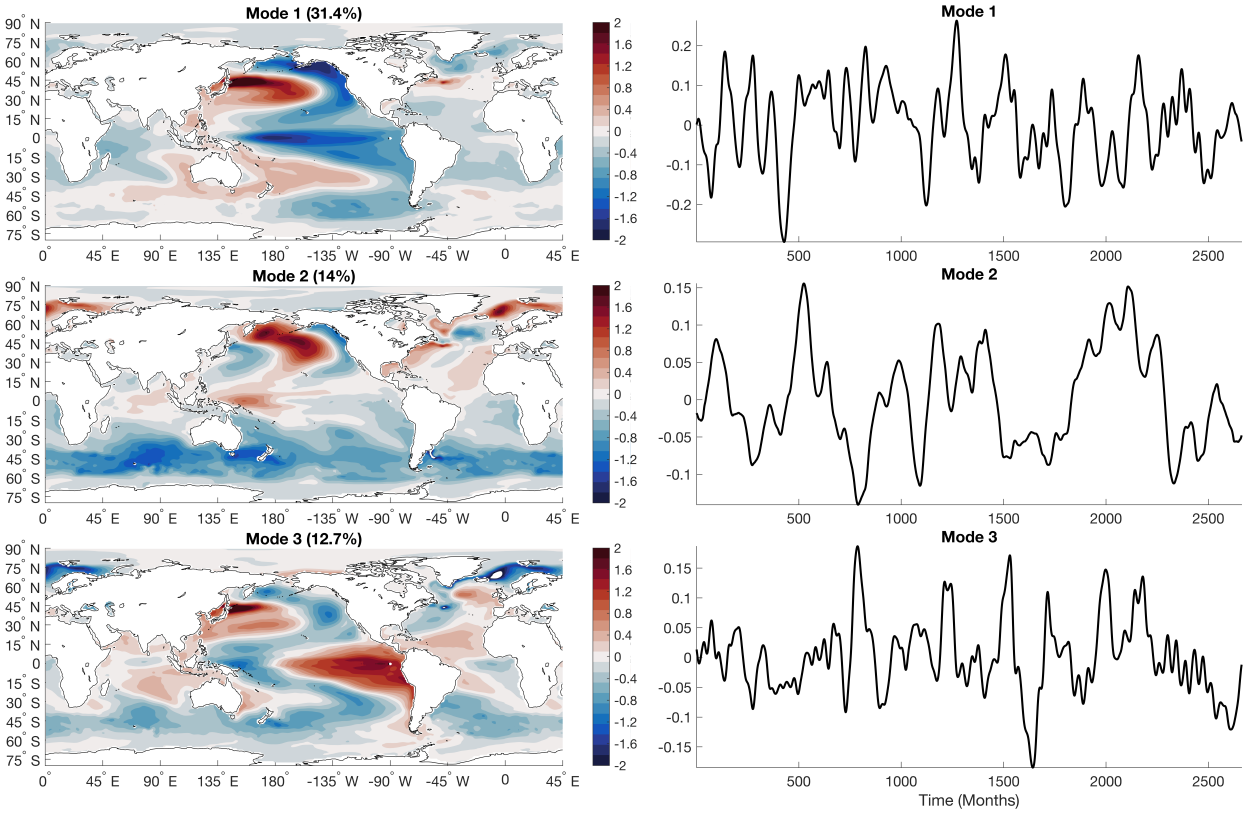

Figure 9: The spatial and temporal patterns for the first (top), second (middle), third (bottom) EOFs of monthly SST anomalies from a 200-year control run using CESM. The three modes explain 31.7%, 13.8%, and 12.8% of the variance, respectively.

Kosaka and Xie (2013) suggest that the pattern in the Pacific Ocean is a natural mode of climate variability resembling La Niña-like decadal cooling, which has further been linked as the cause of

the global warming hiatus. Controlled simulations have shown significant regional and seasonal effects such as an enhanced Walker circulation and weakening of the Aleutian low due to the Pacific-North American (PNA) pattern during boreal winter on a decadal time scale (Chen and Wallace, 2015; Kosaka and Xie, 2013). In combination with the ENSO-related pattern, aspects of the Pacific Decadal Oscillation (PDO) is seen in the North Pacific Ocean (Chen and Wallace, 2015). Tropical Pacific SST anomalies associated with ENSO induce tropical precipitation that forces global atmospheric teleconnections, such as near-surface air temperature, humidity, and winds (Trenberth et al., 1998). The subsequent changes in heat, momentum, and freshwater fluxes induce variations in SST and ocean circulations—thus, ENSO creates an atmospheric bridge connecting the equatorial Pacific to the North Pacific Ocean (Alexander et al., 2002; Lau and Nath, 1994).

The second and third EOF explain 13.8% and 12.8% of the variance respectively. Both display a temporal pattern exhibiting interannual to multi-decadal variability, with larger variations in the third EOF. The spatial pattern corresponding to the second EOF shows the greatest warming in the North Pacific Ocean and the high latitudes of the North Atlantic Ocean. There is a prominent band of variability in the Southern Ocean. Lastly, the third EOF spatial pattern has maximum variability in the northwest and tropical eastern Pacific Ocean, consistent with ENSO-like interdecadal variability. Located adjacent to the equatorial region of anomalously warm SST, a region of opposite sign exists about the equator that creates hemispheric symmetry. Chen and Wallace (2015) suggest that PDO reinforces strong equatorial symmetry that is seen in the first and third EOF.

The similarity of the second EOF from SODAsi.3 and the first EOF from CESM suggests that the dominant pattern in the tropical Pacific Ocean is an internal mode of La Niña–like decadal cooling that plays a role in the tightly coupled ocean-atmosphere system. Furthermore, responses from this tropical forcing result in variations in the extratropics and midlatitudes through the atmospheric bridge (Alexander et al., 2002). To further understand the effects of this internal mode of climate variability, regression maps of the meridional mass streamfunction (MMS), zonal wind velocity, omega, surface currents, and sea level pressure onto the principle component

of the second EOF are examined.

4.1.2.1 Regression maps

Given that longitudinal and meridional SST gradients are crucial to investigating atmospheric circulations, MMS is projected onto the second principle component of SST to create a regression map (Figure 10). The regression closely resembles the pattern of MMS in the second Joint EOF, with some minor differences (Figure 7). The distinction exists in the SH Hadley cell, where the regression identifies two independent negative circulations and the second Joint EOF combines the two circulations. The regression also exhibits a greater magnitude of both SH and NH Hadley cells, with the SH Hadley cell strength concentrated in the lower troposphere. Furthermore, the circulation associated with the Walker circulation is weaker in the regression map than in the Joint EOF. With most of the spatial pattern retained in both the regression map and the second Joint EOF, it can be concluded that there is an expansion of the Hadley cell that is related to the spatial structure of SST in the second EOF.

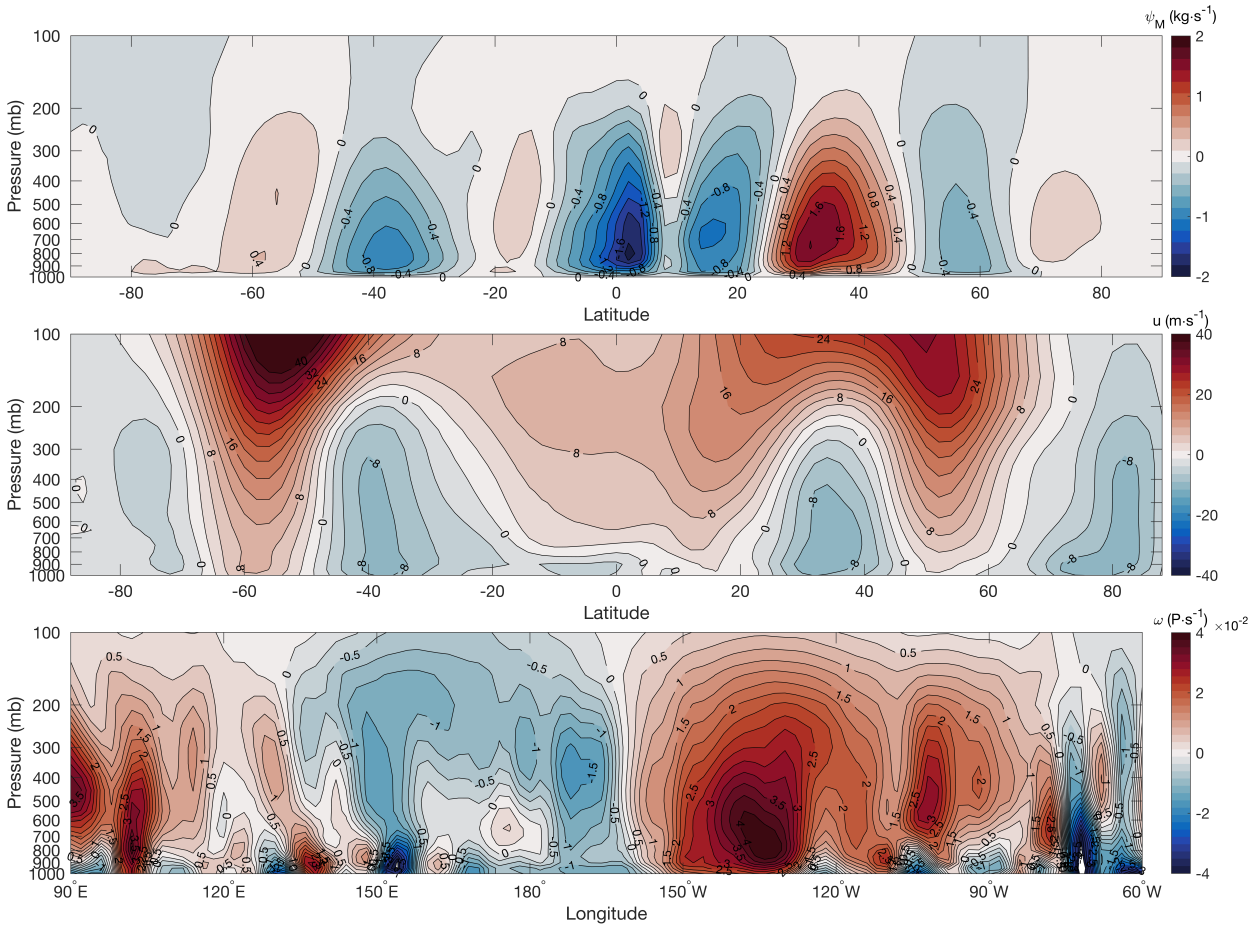

Figure 10: (MMS (top), zonal wind (middle), and omega(bottom) regressed onto the temporal component of SST from the second EOF. Contour interval is 3 $\times$ 10^9 kg $\cdot$ s $^{-1}$ (top), 4 m$\cdot$s^{-1} (middle), and 0.2 P $\cdot$ s^{-1} (bottom).

Since the second Joint EOF of P$-$E establishes the position of the ITCZ, a connection can be created between the meridional SST gradient and MMS. The location of the ITCZ resides in the area where SST is at its maximum, surface winds are at a minimum, and is at the ascending branch of the SH Hadley cell. In addition to the position of the ITCZ located at the ascending branch of the Hadley cell, it is also found where near-surface meridional mass flux and atmospheric energy transport vanishes, which is influenced by ENSO-like patterns on interannual time scales (Adam et al., 2016). These features can be identified using the second EOF of SST with wind stress and the regression map of MMS.

A combination of a northward displaced ITCZ and the longitudinal/latitudinal extent of SST contribute to hemispheric asymmetry. Hemispheric asymmetry creates an imbalance of heat and momentum fluxes across hemispheres that results in the global system redistributing energy and circulations to compensate for the imbalance (Lindzen and Hou, 1988). In this case, the discrepancy leads to the SH Hadley cell to be stronger than the NH Hadley cell (Figure 7). To compensate for the imbalance, the meridional distribution of the global atmospheric circulation varies and is expressed as the differences in magnitude of the subtropical jets across hemispheres (Kessler and Taft, 1987). With a stronger SH Hadley circulation, a stronger Southern Hemisphere subtropical jet is expected. This pattern exists in the regression map of zonal wind velocity associated with the second EOF of SST (Figure 10). The distribution of the zonal wind is divided into two broad regimes—strong westerly jet streams in the upper troposphere between 300-100 mb and weak easterly components in the lower troposphere. In solstitial seasons, the stronger of the two jets will be located poleward of strong trade winds and cross-equatorial flow in the upper troposphere in the winter hemisphere (Webster, 2004). With the typical JJA MMS structure similar to the Hadley circulation, the location of the enhanced westerly jet stream is located in the Southern Hemisphere, further implicating hemispheric asymmetry due to the imbalance of heat.

In addition to the magnitude, the location of the zonal wind can also indicate the latitudinal extent and intensity of the Hadley circulation. In the upper troposphere where friction is negligible, the u-momentum advection is balanced by the Coriolis force and nonlinear advection. This balance suggests that stationary and transient eddies play a role in maintaining the Hadley circulation (Cook, 2004). Hadley cell intensity has been linked to the gradient of latent heat release driven by gradients in SST. Heat is transported from the tropics to the subtropics through transient eddies, indicating that SST gradients influence baroclinic instability and eddy forcing (Rind and Perlwitz, 2004). Likewise to a stronger SH subtropical jet due to an intensified Hadley cell, the surface winds also suggest there is an expansion of the circulation since easterlies extend beyond the tropics, surpassing 40° in both hemispheres (Figure 10). Thus, diabatic circulations and eddy forcing can also modulate the latitudinal extent of the Hadley circulation and further

impact the maintenance of the Ferrell circulation and the subtropical jets (Rind and Perlwitz, 2004).

Following an in-depth examination of atmosphere circulation responses to meridional SST gradients, the longitudinal structure of SST is investigated. The longitudinal pattern of SST in the Pacific Ocean not only influences the strength of the Hadley cells but it also effects the variability and strength of the Walker circulation. With a cooler than normal eastern Pacific Ocean and warmer western Pacific Ocean, an intensified Walker circulation is expected—akin to what happens during La Niña. Wang (2004) found that as a result of an anomalously cold eastern Pacific Ocean, the Pacific Walker circulation, the western Pacific Hadley circulation, and the Atlantic Hadley circulation are strengthened, whereas the eastern Pacific Hadley circulation is weakened. Here, we see a similar structure where there is strong descending motion in the eastern Pacific Ocean but weaker rising motion in the western Pacific Ocean depicted by a regression map of omega (Figure 10). Omega is a derived atmospheric variable defined as the rate of change of pressure with respect to time, and is often used in the atmospheric sciences as an analog for synoptic-scale adiabatic vertical motions, with positive values associated with ascent and negative values associated with sinking motions. These aforementioned rising and sinking motions are consistent with the spatial pattern of MMS and P$-$E in the second Joint EOF (Figure 7). There is an interplay of zonal and meridional circulations in the atmosphere. For example, an intensified zonal circulation strengthens the eastern Pacific Hadley cell and weakens the western Pacific Hadley circulation. In contrast, an intensified Pacific Hadley cell enhances sinking motion of the Walker circulation in the eastern Pacific Ocean and reduces the ascending motion of the Walker circulation. There is a complicated interaction between Hadley cell strength and width, the Walker circulation, and the zonal and meridional structure of SST in the Pacific Ocean. Moreover, SST meridional gradients remain as the main modulators in atmospheric circulations, with longitudinal gradients being of secondary importance (Rind and Perlwitz, 2004). The regression maps of MMS, zonal wind, and omega establish changes in the atmospheric circulation that correspond to the second EOF of SST.

Since prevailing surface winds are a major driving force of ocean currents, the surface currents of the second EOF of SST is investigated (Figure 11). The greatest magnitude shown in the currents occurs in the tropical Pacific Ocean, specifically at the northern edge of the western Pacific warm pool. This pattern represents eastward flow known as the North Equatorial Countercurrent (NECC), which is located below the ITCZ. The notably large current response to SST suggests hemispheric asymmetry of both SST and Hadley circulation and implications of the WES feedback (Chang, 1995). Adjacent to the NECC, westward flows reside on both sides of the equator. The currents located just south of the NECC are stronger than its counterpart north of the NECC but not significantly. This type of pattern is consistent with the WES feedback, where anomalous cross-equatorial flow is deflected by the Coriolis force in both hemispheres. As a result, winds are decreased in the hemisphere where the positive SST anomaly exists (Chang et al., 2006). As the surface winds converge at the ITCZ, wind-driven surface currents such as those seen in Figure 6 are expected. Together, the wind and current ocean variability support an asymmetric SST and Hadley cell pattern.

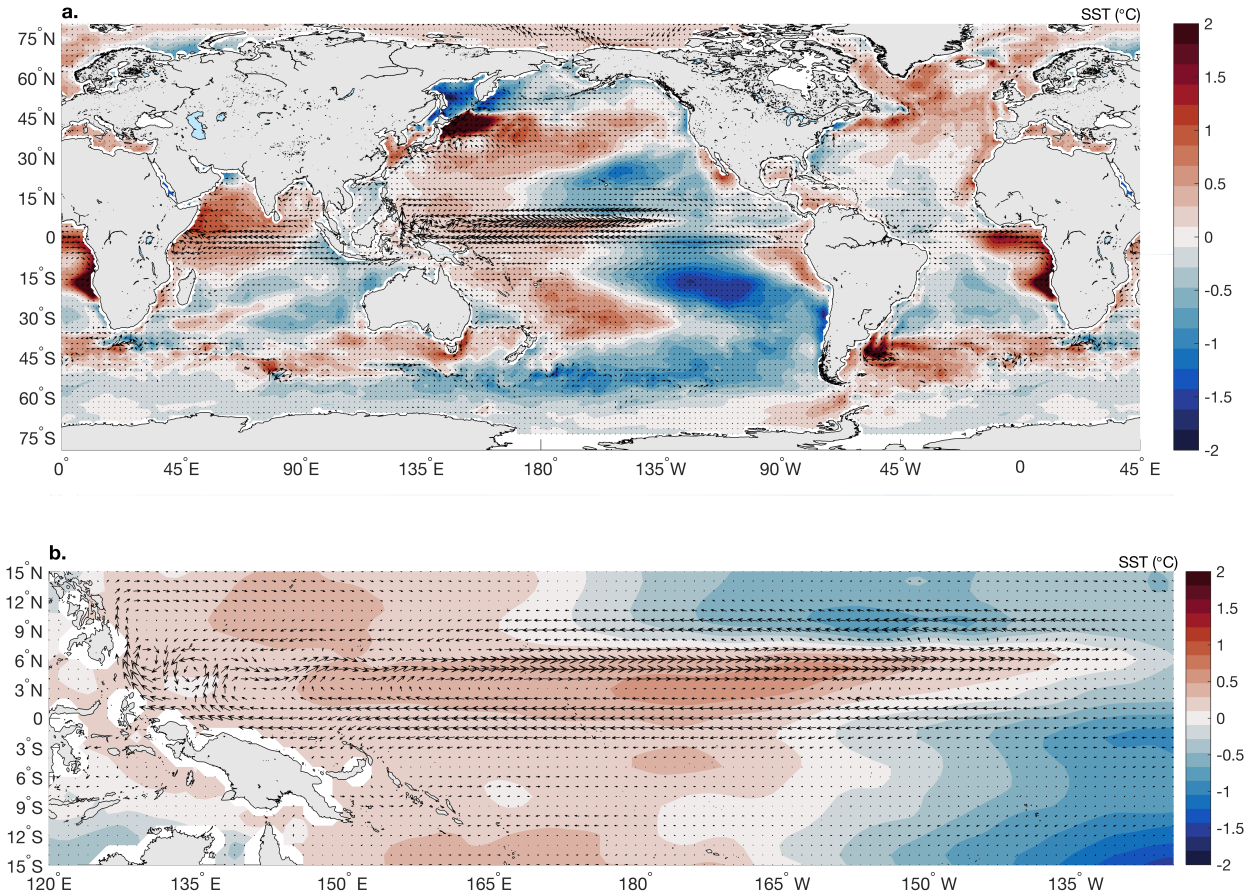

Figure 11: The spatial pattern of the second EOF of SST for the global oceans (a) and Pacific Ocean (b) from SODAsi.3 from 1851-2013. Surface currents regressed onto the second principle component of SST are shown as vectors.

4.1.2.2 The atmospheric bridge

On decadal time scales, there is stronger coupling between the tropics and extra-tropics given the fact that the Bjerknes feedback and dominant SLP patterns occur at these scales (Chen and Wallace, 2015). Additionally, Chen and Wallace (2015) found that interdecadal ENSO-variability exhibits SST signals in the subtropics and extratropics which resembles responses in the PNA pattern—a connection that is consistent with the prominent SLP signature over the Gulf of Alaska. To further understand the implications of decadal variability in the NH Hadley circulation, regression of SLP onto the temporal component of the second EOF of SST is conducted. With similar results as Chen and Wallace (2015), we find high-pressure anomalies

linked to anti-cyclonic wind pattern located in the North Pacific, a common feature of a negative phase of PNA during the boreal winter (Figure 11). The anomalous high pressure is reinforced by the descending branch of the Hadley cell (Figure 6). During La Niña events, the resulting SLP pattern exhibits a weaker than normal Aleutian low over the northeastern Pacific Ocean which results in teleconnections across the North American continent (Gershunov and Barnett, 1998). This includes a significant anti-correlation between the PNA and the NAO connecting the Pacific and Atlantic Oceans through the atmospheric bridge (Alexander et al., 2002; Lau and Nath, 1996; Pinto et al., 2010).

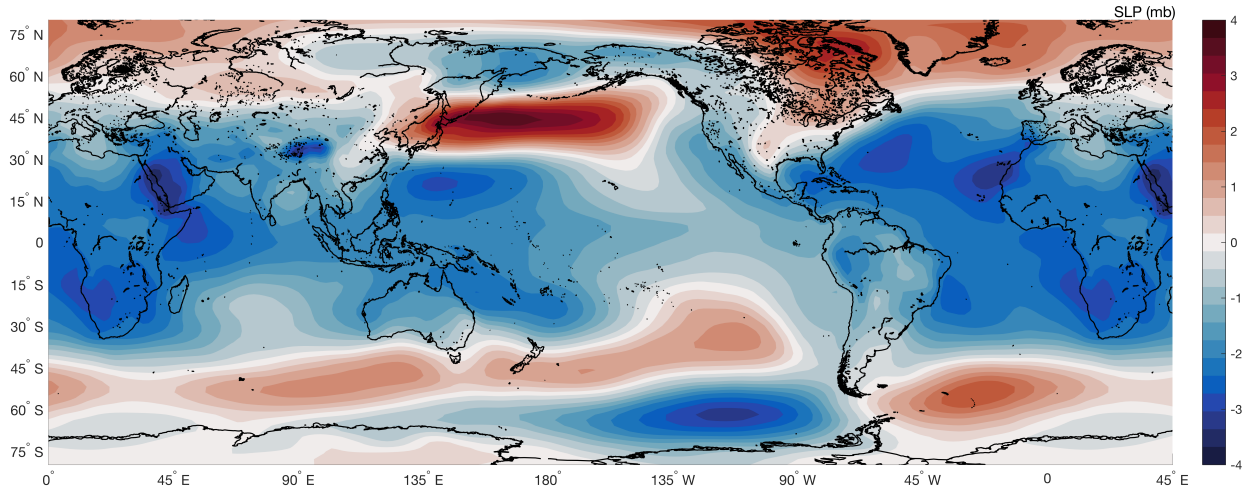

Figure 12: The Mean SLP regressed onto the temporal component of SST from the second EOF. The contour interval is 0.2 mb.

The physical mechanisms connecting the PNA and NAO through the atmospheric bridge involve the downstream wave propagation of low-frequency planetary waves. For example, the negative phase of the PNA pattern exhibits an atmospheric ridge or an anomalous high-pressure system. The ridge modifies the downstream propagation of waves, such as triggering another quasi-stationary Rossby wave train, that results in anticyclonic wave breaking and a positive phase of NAO over the North Atlantic Ocean (Drouard et al., 2015). Furthermore, during a La Niña event, persistent ridging related to the negative phase of PNA deflects the Pacific jet

poleward. As a result, the zonal mean flow induces a meridional tilt to the eddies entering the Atlantic sector that also favors anticyclonic wave breaking and positive NAO (Li and Lau, 2012). This is consistent with the regression map of SLP (Figure 12).

Recent studies have explained AMOC variability through NAO forcing with a response time of the ocean ranging from 5 to 10 years. For example, a positive phase of the NAO strengthens AMOC through heat extraction at the subpolar gyre—subsequently increasing the rate of deep-water formation and horizontal density gradients (Delworth and Zeng, 2016). To establish a connection of decadal changes in SST to AMOC and NAO, the time series of each component is correlated against the second EOF of SST (Figure 13). Consistent with the findings of Giese et al. (2016), a correlation analysis establishes that temporal structure of SST and the North Atlantic meridional streamfunction are correlated (0.70) and further identifies a shift in SST leading the streamfunction by 9 years. An additional correlation analysis using the time series between the second EOF of SST and the NAO index shows that both time series are correlated (0.68), with SST leading NAO by 19 months. Together, the correlation analyses establish a relationship between temperature, NAO, and AMOC. Given that temperature leads atmospheric changes in the Atlantic sector, it is proposed that tropical Pacific SST modulates NAO forcing that subsequently drive AMOC variability.

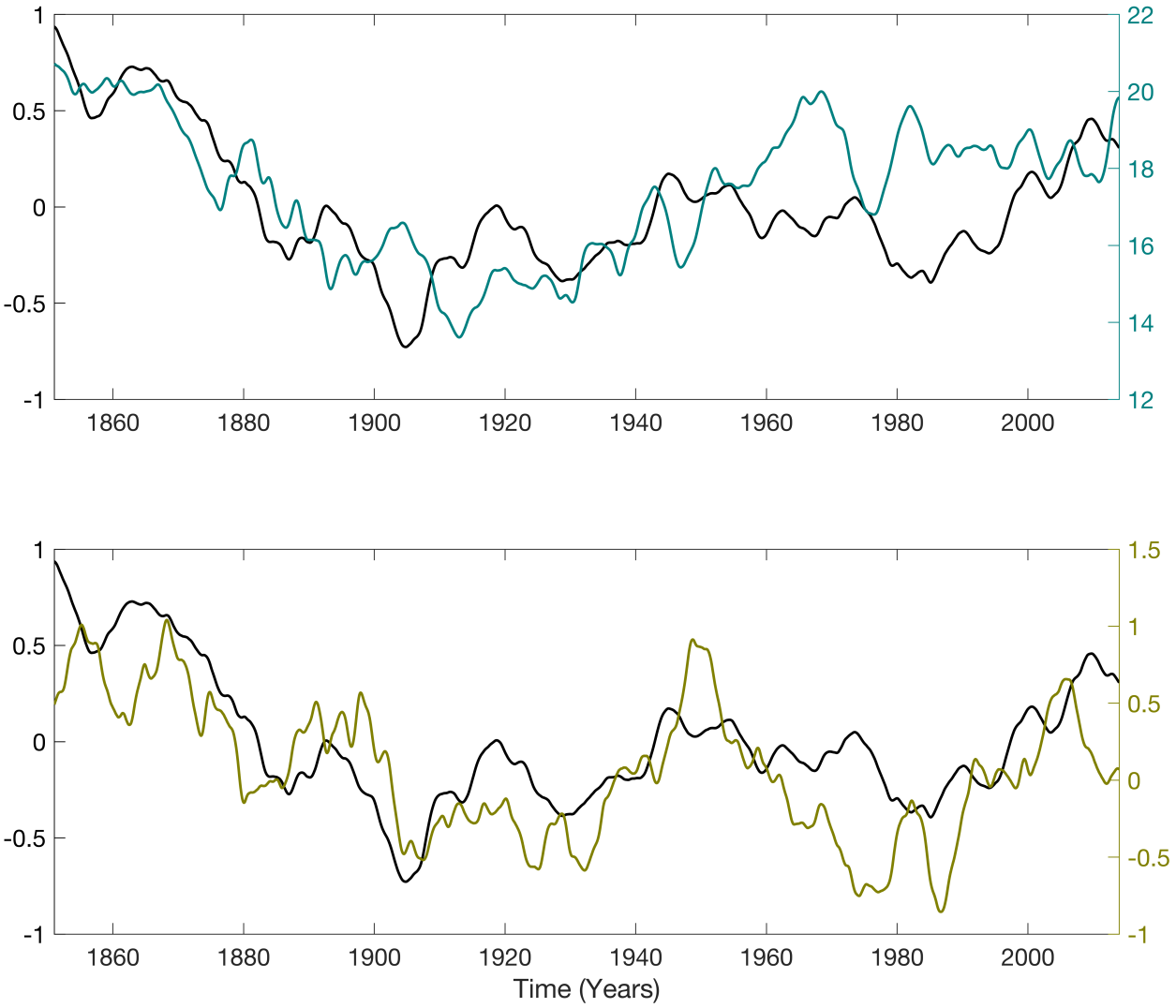

Figure 13: The time series component of the second EOF using SST from SODA shown in black. (Top) The time series of the meridional overturning circulation (Sv); and (bottom) the index of the North Atlantic Oscillation. All time series were smoothed with a 5-year boxcar average.

Figure 14 shows further analysis of the North Atlantic Ocean through the regression of salinity and density anomalies onto the temporal component of the second EOF of SST and the NAO index. Similarities between SST and NAO regression maps is shown by the northern extent of the Gulf Stream that moves along the eastern United States seaboard into the high latitudes of the North Atlantic. Along the coast, there is anomalously cold SST concurrent with elevated values of ocean density. The differences are located along the western boundary near Nova Scotia, where

the spatial extent of the positive salinity and density anomalies that appear at 45°N are larger in the SST regression map. An associated cyclonic wind pattern is located over this region and is consistent with Ekman upwelling over the mid-Atlantic. It appears that large scale wind patterns create density anomalies relating to Ekman pumping. For the NAO regression map, there is an anticyclonic wind pattern thats consistent with a positive phase of NAO.

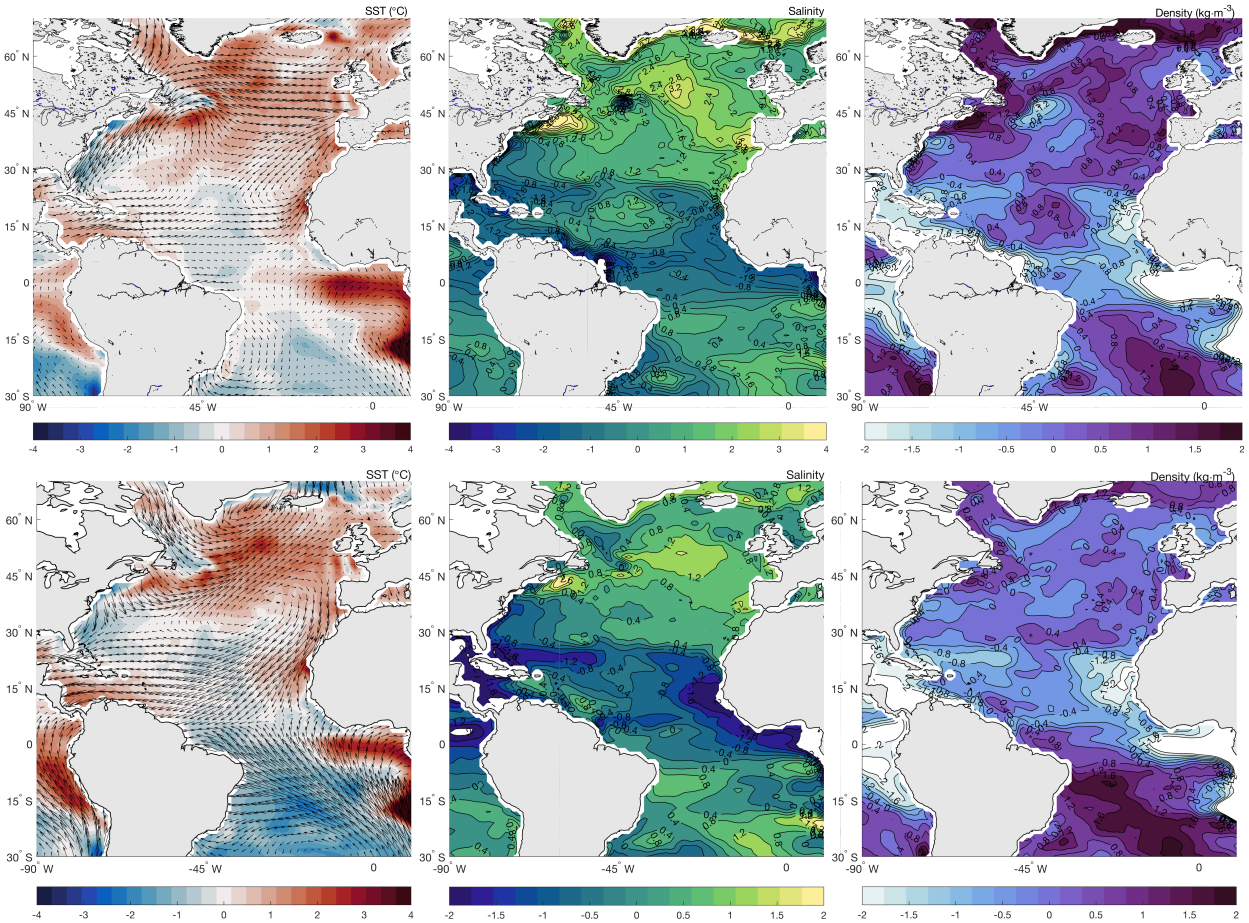

Figure 14: (Top) The North Atlantic Ocean regression maps for the temporal components of the second EOF of SST (top) and the NAO index (bottom). (Top-left) the second EOF of SST with wind stress; (bottom-left) the second EOF of SST and wind stress regressed upon the NAO index; (middle) regression map of salinity anomalies upon the temporal component of the second EOF of SST; (right) regression map of density anomalies upon the temporal component of the second EOF of SST. (Bottom) The North Atlantic Ocean regression maps for the NAO i.

A similar structure seen is reported by Polo et al. (2014) who show density anomalies with southwestward propagation due to Rossby waves migrating along the western boundary. Polo et al. (2014), found several processes important for wind-generated density anomalies, which consequently affect the geostrophic AMOC transport at 26°N. One of these processes is locally generated density anomalies due to coastal upwelling. Another is density anomalies generated remotely as a result of prevailing large-scale wind anomalies located over the mid-Atlantic, typically at a 3-7-year frequency band. Thus, buoyancy-driven decadal variability of AMOC is related to NAO—where NAO leads changes in deep-water formation over the Labrador Sea (Delworth and Greatbatch, 2000). A positive NAO pattern increases heat loss at the surface, resulting in an increase of density over the Labrador Sea that further enhances deep formation linked to the sinking motion of AMOC. To complete the ocean adjustment, density anomalies associated with a NAO-like pattern propagate equatorward along the western boundary of North America. Since this is consistent with the correlation analysis and regression maps of salinity and density, it suggests that SST modulates the atmospheric circulation over the North Atlantic Ocean and indirectly affects AMOC through wind forcing.

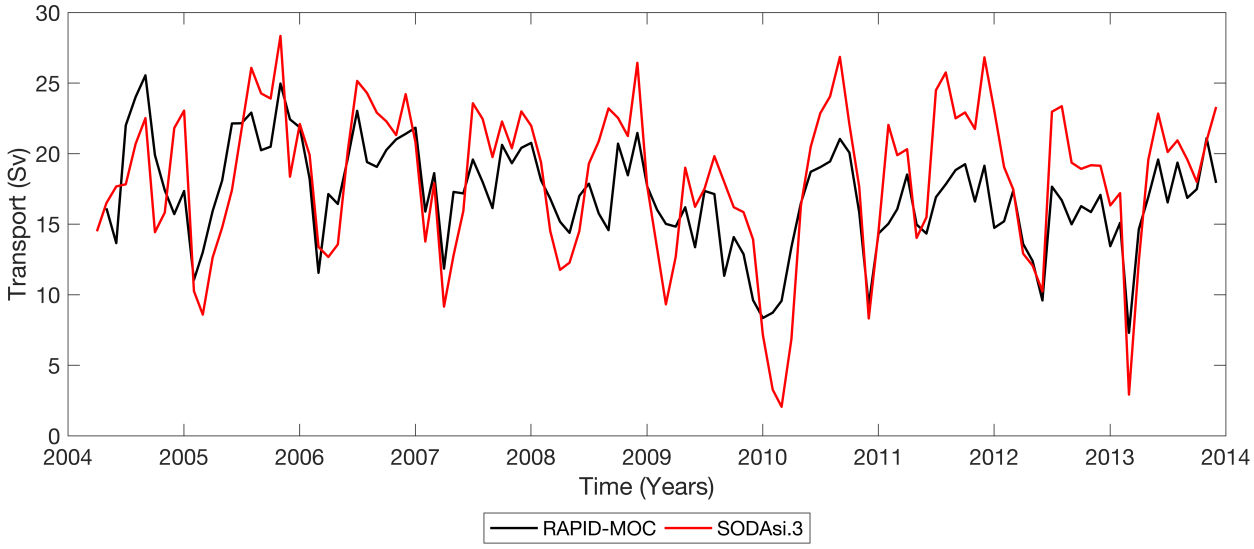

Figure 15: The time series of the meridional overturning circulation (Sv) from RAPID mooring array (black) and SODAsi.3 (red) from 2004 to 2013. Data from the RAPID-MOCHA monitoring project is provided Smeed et al. (2017)

To verify findings from Figures 13 and 14, the MOC transport at 26°N from SODAsi.3 is compared with observations from the RAPID mooring array from 2004-2013 (Figure 15). A correlation analysis between the model and observations determined the data to be correlated at 0.75. Furthermore, the results from second EOF of SST in SODA, the first EOF of SST in CESM, the regression maps, and correlation analysis, we propose that decadal variations in the Northern Hemisphere atmospheric circulations are forced by natural variability in SST that force changes in AMOC.

5. SUMMARY AND CONCLUSION

To further identify physical mechanisms linking decadal variability in SST and AMOC, EOF analyses and regression maps were presented using three different models: SODAsi.3, CESM, and 20CRv2c. The SST fields from SODAsi.3 show variability on time scales ranging from trends to interannual to decadal. The pronounced trend in SST exhibits a spatial pattern of generally increasing global temperature, with some important regions of cooling. These regions include the tropical central Pacific Ocean, the tropical eastern Pacific and Atlantic Oceans, and the Southern Ocean.

In addition to a trend, the EOF analysis of SST shows that there is significant interannual to multi-decadal variability. The second EOF exhibits a distinct spatial pattern, with longitudinal asymmetry illustrated by a warmer western Pacific Ocean and cooler eastern Pacific Ocean. Asymmetry also exists around the equator, creating an inter-hemispheric pattern consisting of a warmer Northern Hemisphere and cooler Southern Hemisphere. The temporal component of the second EOF is correlated with the meridional overturning streamfunction located in the North Atlantic Ocean. SST is found to lead changes in the streamfunction by 9 years.

To distinguish between internal and external forcing related to SST, an experimental preindustrial control run using CESM was used. An EOF analysis of SST shows a pattern resembling a La Niña-like structure that dominates the central Pacific Ocean and is symmetrical across hemispheres. This mode of variability arises from intrinsic variability.

A Joint EOF of SST, the MMS, and P$-$E shows structures associated with the trend and decadal variability that exist in the first and second EOF of SST. The meridional gradient of SST present in the first EOF is reflected in the spatial pattern of MMS. The NH Hadley cell expands across the equator, dominating the tropical atmospheric circulation. With the NH Hadley cell expanding into the Southern Hemisphere and the addition of a strong SH Ferrell circulation, the resulting SH Hadley circulation is weak and contracted. This is also seen in P$-$E, as the ITCZ exists at the ascending branch of the SH Hadley cell. The second Joint EOF shows the SH Hadley

cell dominating the equator as seen by a persistent negative circulation. Located adjacent to the circulation, in the Northern Hemisphere, there is a corresponding negative circulation representing the Walker circulation. Increased P−E is consistent with a strengthened Walker circulation, with increased convection in the western Pacific Ocean and increased subsidence in the eastern Pacific Ocean. An expanded NH Hadley circulation is located poleward of the Walker circulation, exceeding the mean latitudinal extent of the cell. In the extratropics, elevated evaporation is consistent with the descending branches of the NH and SH Hadley cell.

The regression map of MMS onto the temporal component of the second EOF of SST resembles similar results from the second Joint EOF, with the exception of an increase in the magnitude of both the NH and SH Hadley cells and the SH consisting of two separate negative circulations. Together, the wind stress and regression map of MMS indicate that meridional gradients of SST are important in Hadley cell dynamics. Hemispheric differences in the Hadley circulation is also shown by the regression map of zonal wind velocity. Since the SH Hadley cell is stronger than its counterpart, the subtropical jet is stronger in the Southern Hemisphere. The latitudinal extent of each cell is indicated by the presence of low-level easterlies in the tropics. There are broad easterlies that cross the equator in the Southern Hemisphere and a narrow band of easterlies in the Northern Hemisphere. This is consistent with an expanded SH Hadley cell and poleward shift in the NH Hadley cell. Additionally, the wind-driven surface currents echoes the hemispheric asymmetry in SST and the Hadley circulation. This is seen in an increased NECC located at the narrow warm pool, below the ITCZ, in the tropical Pacific Ocean.

In further investigating the impact of SST gradients on atmospheric circulations, the regression map of omega illustrates that the longitudinal gradient of SST influences zonal atmospheric circulations. The Walker circulation is clearly identified. The descending branch of the circulation is located at 135°W and the ascending branch is located at approximately 160°E, where the descending motion is robust. The intensity and latitudinal extent of the Hadley circulation is further impacted by an elevated Walker circulation.

A time series containing seasonal means of the latitudinal extent of the NH and SH Hadley

circulation demonstrates Northern Hemisphere decadal variability and a pronounced trend in the Southern Hemisphere. Relating results found in the EOF analyses of SST from SODA and CESM with the time series of the latitudinal extent suggests that the Southern Hemisphere corresponds to externally forced SST whereas the Northern Hemisphere is similar to La Niña-like internal variability. Decadal variability in the Northern Hemisphere modifies atmospheric circulations in the North Pacific and Atlantic Oceans through the atmospheric bridge. A regression map of SLP reveals a ridge of a high-pressure anomaly in the North Pacific Ocean. This indicates a weakened Aleutian Low, which is a pattern that occurs during the positive phase of the PNA. The ridge is located in the North Pacific Ocean and can influence atmospheric circulation in the North Atlantic through modification of wave propagations downstream that result in a positive phase of NAO. The wind stress associated with the second EOF of SST exhibit anticyclonic flow that's consistent with the positive phase of NAO.

The time series of the second EOF of SST and NAO index are correlated, as shown by a correlation analysis, with SST leading changes in the atmospheric circulation by 19 months. In addition, a correlation was found between SST and AMOC such that SST leads changes in the circulation by 9 years. Together, we propose that tropical Pacific Ocean SST modifies atmospheric circulations located over the North Atlantic Circulation. The resulting wind stress pattern forces heat exchanges between the atmosphere and ocean. The exchange induces a change in density anomalies along the western boundary of the North Atlantic Ocean basin. To complete the ocean adjustment, these anomalies migrate southwestward along the boundary through wave propagations. The perturbation subsequently affects AMOC transport at 26° that is typically seen by the RAPID mooring array.

The analysis shows that there are two dominate modes of variability. The first mode is largely an increase in the trend of global temperatures that is presumed to be of anthropogenic origin. This mode is revealed in the Southern Hemisphere. The SST spatial pattern of the first EOF displays a larger temperature gradient in the Southern Hemisphere than in the Northern Hemisphere, indicating SST modulates atmospheric circulations in the Southern Hemisphere. The

regression of winds and MMS onto the temporal component of SST further explains southward shift of the Hadley circulation in the Northern Hemisphere. However, the Southern Hemisphere presents strong winds stresses over the Southern Ocean that represents a strengthened Ferrell circulation as seen in MMS. Since the Ferrell circulation is an indirect cell, the large meridional temperature gradient in the Southern Hemisphere SST pattern is modulating its strength.

The second mode exhibits decadal variability and is seen in the Northern Hemisphere, as explained by variability in the latitudinal extend of the NH Hadley cell. The EOF analysis of CESM illustrates decadal variability with spatial features similar to that of the second EOF of SST from SODA. Furthermore, it is proposed that this mode in SODA is modulated by internal variability of SST of the tropical Pacific Ocean. The regression of MMS explains that the atmospheric circulation associated with this mode exhibits greater intensity of the Hadley cell in the Northern Hemisphere. The intensity of the Hadley cell is linked with an expansion of the latitudinal extent of the cell. With this structure, the pressure systems are modified as a result of the intensity and extent of MMS. These pressure systems, combined with the Hadley circulation, influence atmospheric circulations over the Atlantic Ocean through the atmospheric bridge. Here, the tropical Pacific Ocean forces changes over the North Atlantic Ocean through the North Atlantic Oscillation. Wind forcing associated with NAO at interannual frequencies modulate local and remote density anomalies through heat exchange between the ocean and atmosphere. These density anomalies then propagate along the coast of the eastern seaboard of the United States to impact the strength of AMOC at the entrance of the Gulf Stream. The progression of events indicate the Northern Hemisphere is exhibiting decadal variability that is in both SST and AMOC. This variability lags changes in SST but leads changes in AMOC, therefore it is presumed that the SST pattern in the tropical Pacific Ocean is regulating atmospheric circulations in the Northern Hemisphere that force AMOC.

REFERENCES

Adam, O., Bischoff, T., and Schneider, T. (2016). Seasonal and interannual variations of the energy flux equator and itcz. part i: Zonally averaged itcz position. *Journal of Climate*, 29(9):3219–3230.

Alexander, M. A., Bladé, I., Newman, M., Lanzante, J. R., Lau, N.-C., and Scott, J. D. (2002). The atmospheric bridge: The influence of enso teleconnections on air–sea interaction over the global oceans. *Journal of Climate*, 15(16):2205–2231.

Bentsen, M., Drange, H., Furevik, T., and Zhou, T. (2004). Simulated variability of the atlantic meridional overturning circulation. *Climate Dynamics*, 22(6-7):701–720.

Biastoch, A., Böning, C. W., and Lutjeharms, J. R. E. (2008). Agulhas leakage dynamics affects decadal variability in atlantic overturning circulation. *Nature*, 456(7221):489–492.

Böning, C. W., Scheinert, M., Dengg, J., Biastoch, A., and Funk, A. (2006). Decadal variability of subpolar gyre transport and its reverberation in the north atlantic overturning. *Geophysical Research Letters*, 33(21).

Bower, A. S., Lozier, M. S., Gary, S. F., and Böning, C. W. (2009). Interior pathways of the north atlantic meridional overturning circulation. *Nature*, 459(7244):243–247.

Buckley, M. W., Ferreira, D., Campin, J.-M., Marshall, J., and Tulloch, R. (2012). On the relationship between decadal buoyancy anomalies and variability of the atlantic meridional overturning circulation. *Journal of Climate*, 25(23):8009–8030.

Buckley, M. W. and Marshall, J. (2016). Observations, inferences, and mechanisms of the atlantic meridional overturning circulation: A review. *Reviews of Geophysics*, 54(1):5–63.

Carton, J. A. and Giese, B. S. (2008). A reanalysis of ocean climate using simple ocean data

assimilation (soda). *Monthly Weather Review*, 136(8):2999–3017.

Chang, E. K. M. (1995). The influence of hadley circulation intensity changes on extratropical climate in an idealized model. *Journal of the Atmospheric Sciences*, 52(11):2006–2024.

Chang, P., Yamagata, T., Schopf, P., Behera, S. K., Carton, J., Kessler, W. S., Meyers, G., Qu, T., Schott, F., Shetye, S., and et al. (2006). Climate fluctuations of tropical coupled systems—the role of ocean dynamics. *Journal of Climate*, 19(20):5122–5174.

Chen, X. and Wallace, J. M. (2015). Enso-like variability: 1900–2013*. *Journal of Climate*, 28(24):9623–9641.

Chiang, J. C. H. and Bitz, C. M. (2005). Influence of high latitude ice cover on the marine intertropical convergence zone. *Climate Dynamics*, 25(5):477–496.

Compo, G. P., Whitaker, J. S., and Sardeshmukh, P. D. (2006). Feasibility of a 100-year reanalysis using only surface pressure data. *Bulletin of the American Meteorological Society*, 87(2):175–190.

Compo, G. P., Whitaker, J. S., Sardeshmukh, P. D., Matsui, N., Allan, R. J., Yin, X., Gleason, B. E., Vose, R. S., Rutledge, G., Bessemoulin, P., and et al. (2011). The twentieth century reanalysis project. *Quarterly Journal of the Royal Meteorological Society*, 137(654):1–28.

Cook, K. H. (2004). Hadley circulation dynamics. *The Hadley Circulation: Present, Past and Future*, pages 61–83.

Danabasoglu, G. (2008). On multidecadal variability of the atlantic meridional overturning circulation in the community climate system model version 3. *Journal of Climate*, 21(21):5524–5544.

Danabasoglu, G., Bates, S. C., Briegleb, B. P., Jayne, S. R., Jochum, M., Large, W. G., Peacock, S., and Yeager, S. G. (2012). The ccsm4 ocean component. *Journal of Climate*, 25(5):1361–1389.

Danabasoglu, G., Yeager, S. G., Kim, W. M., Behrens, E., Bentsen, M., Bi, D., Biastoch, A., Bleck, R., Böning, C., Bozec, A., and et al. (2016). North atlantic simulations in coordinated ocean-ice reference experiments phase ii (core-ii). part ii: Inter-annual to decadal variability. *Ocean Modelling*, 97:65–90.

Delworth, T., Manabe, S., and Stouffer, R. J. (1993). Interdecadal variations of the thermohaline circulation in a coupled ocean-atmosphere model. *Journal of Climate*, 6(11):1993–2011.

Delworth, T. L. and Fanrong, Z. (2012). Multicentennial variability of the atlantic meridional overturning circulation and its climatic influence in a 4000 year simulation of the gfdl cm2.1 climate model. *Geophysical Research Letters*, 39(13).

Delworth, T. L. and Greatbatch, R. J. (2000). Multidecadal thermohaline circulation variability driven by atmospheric surface flux forcing. *Journal of Climate*, 13(9):1481–1495.

Delworth, T. L. and Zeng, F. (2016). The impact of the north atlantic oscillation on climate through its influence on the atlantic meridional overturning circulation. *Journal of Climate*, 29(3):941–962.

Deser, C., Phillips, A. S., Tomas, R. A., Okumura, Y. M., Alexander, M. A., Capotondi, A., Scott, J. D., Kwon, Y.-O., and Ohba, M. (2012). Enso and pacific decadal variability in the community climate system model version 4. *Journal of Climate*, 25(8):2622–2651.

Dong, S., Garzoli, S., and Baringer, M. (2011). The role of interocean exchanges on decadal variations of the meridional heat transport in the south atlantic. *Journal of Physical Oceanography*, 41(8):1498–1511.

Drouard, M., Rivière, G., and Arbogast, P. (2015). The link between the north pacific climate variability and the north atlantic oscillation via downstream propagation of synoptic waves. *Journal of Climate*, 28(10):3957–3976.

Garzoli, S. L. and Matano, R. (2011). The south atlantic and the atlantic meridional overturning circulation. *Deep Sea Research Part II: Topical Studies in Oceanography*, 58(17-18):1837–1847.

Gastineau, G., Li, L., and Le Treut, H. (2009). The hadley and walker circulation changes in global warming conditions described by idealized atmospheric simulations. *Journal of Climate*, 22(14):3993–4013.

Gent, P. R., Danabasoglu, G., Donner, L. J., Holland, M. M., Hunke, E. C., Jayne, S. R., Lawrence, D. M., Neale, R. B., Rasch, P. J., Vertenstein, M., and et al. (2011). The community climate system model version 4. *Journal of Climate*, 24(19):4973–4991.

Gershunov, A. and Barnett, T. P. (1998). Interdecadal modulation of enso teleconnections. *Bulletin of the American Meteorological Society*, 79(12):2715–2725.

Giese, B. S. and Carton, J. A. (1999). Interannual and decadal variability in the tropical and midlatitude pacific ocean. *Journal of Climate*, 12(12):3402–3418.

Giese, B. S., Seidel, H. F., Compo, G. P., and Sardeshmukh, P. D. (2016). An ensemble of ocean reanalyses for 1815-2013 with sparse observational input. *Journal of Geophysical Research: Oceans*, 121(9):6891–6910.

Gulev, S. K., Latif, M., Keenlyside, N., Park, W., and Koltermann, K. P. (2013). North atlantic ocean control on surface heat flux on multidecadal timescales. *Nature*, 499(7459):464–467.

Häkkinen, S. (1999). Variability of the simulated meridional heat transport in the north atlantic for the period 1951-1993. *Journal of Geophysical Research: Oceans*, 104(C5):10991–11007.

Hirschi, J. J.-M., Blaker, A. T., Sinha, B., Coward, A., de Cuevas, B., Alderson, S., and Madec, G. (2013). Chaotic variability of the meridional overturning circulation on subannual to interannual timescales. *Ocean Science*, 9(5):805–823.

Hirschi, J. J.-M., Killworth, P. D., and Blundell, J. R. (2007). Subannual, seasonal, and interannual variability of the north atlantic meridional overturning circulation. *Journal of Physical Oceanography*, 37(5):1246–1265.

Hunke, E. C., Lipscomb, W. H., Turner, A. K., Jeffery, N., and Elliott, S. (2010). Cice: the los alamos sea ice model documentation and software user's manual version 4.1 la-cc-06-012.

Hurrell, J. W., Holland, M. M., Gent, P. R., Ghan, S., Kay, J. E., Kushner, P. J., Lamarque, J.-F., Large, W. G., Lawrence, D., Lindsay, K., and et al. (2013). The community earth system model: A framework for collaborative research. *Bulletin of the American Meteorological Society*, 94(9):1339–1360.

Jones, P. D., Jonsson, T., and Wheeler, D. (1997). Extension to the north atlantic oscillation using early instrumental pressure observations from gibraltar and south-west iceland. *International Journal of Climatology*, 17(13):1433–1450.

Kang, S. M., Polvani, L. M., Fyfe, J. C., and Sigmond, M. (2011). Impact of polar ozone depletion on subtropical precipitation. *Science*, 332(6032):951–954.

Kessler, W. S. and Taft, B. A. (1987). Dynamic heights and zonal geostrophic transports in the central tropical pacific during 1979–84. *Journal of Physical Oceanography*, 17(1):97–122.

Kim, W. M., Yeager, S., Chang, P., and Danabasoglu, G. (2018). Low-frequency north atlantic climate variability in the community earth system model large ensemble. *Journal of Climate*, 31(2):787–813.

Knight, J. R. (2005). A signature of persistent natural thermohaline circulation cycles in observed climate. *Geophysical Research Letters*, 32(20).

Knight, J. R. (2009). The atlantic multidecadal oscillation inferred from the forced climate response in coupled general circulation models. *Journal of Climate*, 22(7):1610–1625.

Kosaka, Y. and Xie, S.-P. (2013). Recent global-warming hiatus tied to equatorial pacific surface cooling. *Nature*, 501(7467):403–407.

Kostov, Y., Armour, K. C., and Marshall, J. (2014). Impact of the atlantic meridional overturning circulation on ocean heat storage and transient climate change. *Geophysical Research Letters*, 41(6):2108–2116.

Kuhlbrodt, T., Griesel, A., Montoya, M., Levermann, A., Hofmann, M., and Rahmstorf, S. (2007). On the driving processes of the atlantic meridional overturning circulation. *Reviews of Geophysics*, 45(2).

Lau, N.-C. and Nath, M. J. (1994). A modeling study of the relative roles of tropical and extratropical sst anomalies in the variability of the global atmosphere-ocean system. *Journal of Climate*, 7(8):1184–1207.

Lau, N.-C. and Nath, M. J. (1996). The role of the "atmospheric bridge" in linking tropical pacific enso events to extratropical sst anomalies. *Journal of Climate*, 9(9):2036–2057.

Lawrence, D. M., Oleson, K. W., Flanner, M. G., Thornton, P. E., Swenson, S. C., Lawrence, P. J., Zeng, X., Yang, Z.-L., Levis, S., Sakaguchi, K., et al. (2011). Parameterization improvements and functional and structural advances in version 4 of the community land model. *Journal of Advances in Modeling Earth Systems*, 3(1).

Li, Y. and Lau, N.-C. (2012). Impact of enso on the atmospheric variability over the north atlantic in late winter—role of transient eddies. *Journal of Climate*, 25(1):320–342.

Lindzen, R. S. and Hou, A. V. (1988). Hadley circulations for zonally averaged heating centered off the equator. *Journal of the Atmospheric Sciences*, 45(17):2416–2427.

Lozier, M. S. (2010). Deconstructing the conveyor belt. *Science*, 328(5985):1507–1511.

Manabe, S., Bryan, K., and Spelman, M. J. (1990). Transient response of a global ocean-

atmosphere model to a doubling of atmospheric carbon dioxide. *Journal of Physical Oceanography*, 20(5):722–749.

Marshall, J., Donohoe, A., Ferreira, D., and McGee, D. (2013). The ocean's role in setting the mean position of the inter-tropical convergence zone. *Climate Dynamics*, 42(7-8):1967–1979.

Marshall, J. and Schott, F. (1999). Open-ocean convection: Observations, theory, and models. *Reviews of Geophysics*, 37(1):1–64.

McCarthy, G., Frajka-Williams, E., Johns, W., Baringer, M., Meinen, C., Bryden, H., Rayner, D., Duchez, A., Roberts, C., and Cunningham, S. (2012). Observed interannual variability of the atlantic meridional overturning circulation at 26.5 n. *Geophysical Research Letters*, 39(19).

Munoz, E., Kirtman, B., and Weijer, W. (2011). Varied representation of the atlantic meridional overturning across multidecadal ocean reanalyses. *Deep Sea Research Part II: Topical Studies in Oceanography*, 58(17-18):1848–1857.

Neale, R. B., Chen, C.-C., Gettelman, A., Lauritzen, P. H., Park, S., Williamson, D. L., Conley, A. J., Garcia, R., Kinnison, D., Lamarque, J.-F., et al. (2010). Description of the ncar community atmosphere model (cam 5.0). *NCAR Tech. Note NCAR/TN-486+ STR*, 1(1):1–12.

Pinto, J. G., Reyers, M., and Ulbrich, U. (2010). The variable link between pna and nao in observations and in multi-century cgcm simulations. *Climate Dynamics*, 36(1-2):337–354.

Polo, I., Robson, J., Sutton, R., and Balmaseda, M. A. (2014). The importance of wind and buoyancy forcing for the boundary density variations and the geostrophic component of the amoc at 26 °n. *Journal of Physical Oceanography*, 44(9):2387–2408.

Quan, X.-W., Diaz, H. F., and Hoerling, M. P. (2004). Change in the tropical hadley cell since 1950. *The Hadley Circulation: Present, Past and Future*, pages 85–120.

Rayner, D., Hirschi, J. J.-M., Kanzow, T., Johns, W. E., Wright, P. G., Frajka-Williams, E.,

Bryden, H. L., Meinen, C. S., Baringer, M. O., Marotzke, J., and et al. (2011). Monitoring the atlantic meridional overturning circulation. *Deep Sea Research Part II: Topical Studies in Oceanography*, 58(17-18):1744–1753.

Rayner, N. A. (2003). Global analyses of sea surface temperature, sea ice, and night marine air temperature since the late nineteenth century. *Journal of Geophysical Research*, 108(D14).

Rind, D. and Perlwitz, J. (2004). The response of the hadley circulation to climate changes, past and future. *The Hadley Circulation: Present, Past and Future*, pages 399–435.

Roberts, C. D., Waters, J., Peterson, K. A., Palmer, M. D., McCarthy, G. D., Frajka-Williams, E., Haines, K., Lea, D. J., Martin, M. J., Storkey, D., and et al. (2013). Atmosphere drives recent interannual variability of the atlantic meridional overturning circulation at 26.5 °n. *Geophysical Research Letters*, 40(19):5164–5170.

Robson, J., Sutton, R., Lohmann, K., Smith, D., and Palmer, M. D. (2012). Causes of the rapid warming of the north atlantic ocean in the mid-1990s. *Journal of Climate*, 25(12):4116–4134.

Rossby, T. (1999). On gyre interactions. *Deep Sea Research Part II: Topical Studies in Oceanography*, 46(1-2):139–164.

Schneider, E. K. and Fan, M. (2012). Observed decadal north atlantic tripole sst variability. part ii: Diagnosis of mechanisms. *Journal of the Atmospheric Sciences*, 69(1):51–64.

Schneider, T., Bischoff, T., and Haug, G. H. (2014). Migrations and dynamics of the intertropical convergence zone. *Nature*, 513(7516):45–53.

Schuster, U. and Watson, A. J. (2007). A variable and decreasing sink for atmospheric co2in the north atlantic. *Journal of Geophysical Research*, 112(C11).

Seager, R., Naik, N., and Vecchi, G. A. (2010). Thermodynamic and dynamic mechanisms for large-scale changes in the hydrological cycle in response to global warming*. *Journal of*

Climate, 23(17):4651–4668.

Smeed, D., McCarthy, G., Rayner, D., Moat, B. I., Johns, W. E., Baringer, M. O., and Meinen, C. S. (2017). Atlantic meridional overturning circulation observed by the rapid-mocha-wbts (rapid-meridional overturning circulation and heatflux array-western boundary time series) array at 26n from 2004 to 2017.

Smith, R., Dukowicz, J., and Malone, R. (1992). Parallel ocean general circulation modeling. *Physica D: Nonlinear Phenomena*, 60(1-4):38–61.

Stouffer, R. J., Yin, J., Gregory, J. M., Dixon, K. W., Spelman, M. J., Hurlin, W., Weaver, A. J., Eby, M., Flato, G. M., Hasumi, H., and et al. (2006). Investigating the causes of the response of the thermohaline circulation to past and future climate changes. *Journal of Climate*, 19(8):1365–1387.

Trenberth, K. E., Branstator, G. W., Karoly, D., Kumar, A., Lau, N.-C., and Ropelewski, C. (1998). Progress during toga in understanding and modeling global teleconnections associated with tropical sea surface temperatures. *Journal of Geophysical Research: Oceans*, 103(C7):14291–14324.

Trenberth, K. E. and Caron, J. M. (2001). Estimates of meridional atmosphere and ocean heat transports. *Journal of Climate*, 14(16):3433–3443.

Vellinga, M. and Wood, R. A. (2002). Global climatic impacts of a collapse of the atlantic thermohaline circulation. *Climatic Change*, 54(3):251–267.

Wang, C. (2004). Enso, atlantic climate variability, and the walker and hadley circulations. *The Hadley Circulation: Present, Past and Future*, pages 173–202.

Washington, W. M. and Meehl, G. A. (1989). Climate sensitivity due to increased co2: experiments with a coupled atmosphere and ocean general circulation model. *Climate Dynamics*, 4(1):1–38.

Webster, P. J. (2004). The elementary hadley circulation. *The Hadley Circulation: Present, Past and Future*, pages 9–60.

Whitaker, J. S. and Hamill, T. M. (2002). Ensemble data assimilation without perturbed observations. *Monthly Weather Review*, 130(7):1913–1924.

Woodruff, S. D., Worley, S. J., Lubker, S. J., Ji, Z., Eric Freeman, J., Berry, D. I., Brohan, P., Kent, E. C., Reynolds, R. W., Smith, S. R., and et al. (2010). Icoads release 2.5: extensions and enhancements to the surface marine meteorological archive. *International Journal of Climatology*, 31(7):951–967.

Xie, S.-P. and Philander, S. G. H. (1994). A coupled ocean-atmosphere model of relevance to the itcz in the eastern pacific. *Tellus A: Dynamic Meteorology and Oceanography*, 46(4):340–350.

Yeager, S. and Danabasoglu, G. (2014). The origins of late-twentieth-century variations in the large-scale north atlantic circulation. *Journal of Climate*, 27(9):3222–3247.

Zhang, L. and Wang, C. (2013). Multidecadal north atlantic sea surface temperature and atlantic meridional overturning circulation variability in cmip5 historical simulations. *Journal of Geophysical Research: Oceans*, 118(10):5772–5791.

Zhang, Y., Wallace, J. M., and Battisti, D. S. (1997). Enso-like interdecadal variability: 1900–93. *Journal of Climate*, 10(5):1004–1020.